Title
Benthic biogeochemical processes related to water column oxygen deficiency in the Santa Monica Basin, North East Pacific Ocean

Author
Lemieux, Sydnie Lynn

Publication Date
2017

Peer reviewed|Thesis/dissertation

UNIVERSITY OF CALIFORNIA

Los Angeles

Benthic biogeochemical processes related to water column oxygen deficiency in the Santa Monica Basin, North East Pacific Ocean

A thesis submitted in partial satisfaction of the
requirements for the degree Master of Science
in Atmospheric and Oceanic Sciences

by

Sydnie Lynn LeMieux

2017

ABSTRACT OF THE THESIS

Benthic biogeochemical processes related to water column oxygen deficiency in the Santa Monica Basin, North East Pacific Ocean

by

Sydnie Lynn Lemieux

Master of Science in Atmospheric and Oceanic Sciences

University of California, Los Angeles, 2017

Professor Tina Irene Treude, Chair

Mid-water oceanic depths in coastal upwelling regions often contain oxygen deficient waters, called oxygen minimum zones (OMZs). These hypoxic (< 60 µM O_2) conditions can have adverse effects on ecosystems, as many organisms cannot survive in low O_2 conditions. This study investigated the OMZ in the topographically isolated Santa Monica Basin (SMB), California, a recipient of high nutrient input. The last survey of this area ~35 years ago, reported a pervious 350 year expansion of the SMB OMZ. In order to assess the OMZ since the last evaluation, sediment cores from 12 stations were retrieved by a multicorer from O_2-ventilated (>60 µM O_2) to near-anoxia (~4 µM O_2) regions along two depth-transects ranging from water depths between 71 and 907 m. The sediment porewater and supernatant water of the cores were analyzed for sulfate (SO_4^{2-}), nitrate (NO_3^-), phosphate (PO_4^{3-}), ammonium (NH_4^+), total sulfide, dissolved iron (Fe (II)), total alkalinity (TA) and bacterial sulfate reduction. The two deepest stations

(907 and 893 meters, ~5 µM O_2) exhibited down-core accumulation of NH_4^+ and TA, while also displaying enhanced rates of sulfate reduction close to the sediment surface; these patterns are all evidence of low oxygen conditions in the overlying water column. Shallower stations upslope (starting at 777 m water depth) featured increasing signs of bioturbation and bioirrigation effects in the geochemical profiles of NH_4^+, TA, PO_4^{3-} and Fe (II). Low sulfate reduction rates (areal rates range from 0.13–0.86 mmol m^{-2} d^{-1}) were detected at all stations. These results were compared with data separate from this thesis, including: ^{210}Pb lamination analyses, the presence and activity of macrofauna at the seafloor, and iron speciation analyses. According to the stations sampled, we could not identify a definite spreading or reduction of the OMZ at the seafloor since the last survey of the SMB was done ~35 years ago.

The thesis of Sydnie Lynn Lemieux is approved.

Daniele Bianchi

Peggy Marie Fong

Will Berelson

Tina Irene Treude, Committee Chair

University of California, Los Angeles

2017

Table of contents

List of Figures

List of Tables

Acknowledgements

I would like to thank Prof. Dr. Tina Treude for supporting this project and her overall mentorship. I am especially grateful for the laughs we shared in the lab and on the boat, the comfort she provided many times, and for her patience with me as I carried out the research and wrote this thesis.

A very special thank you goes to Jeana Drake, who helped immensely in the lab and with analyzing data. Thank you to both Jeana and Tina for pushing me outside my comfort zone whether it was presenting data or in the lab.

I would also like to thank Dr. Will Berelson for his advice, guidance and positive support throughout this project. Dr. Daniele Bianchi and Dr. Peggy Fong also provided great encouragement.

Thank you to Sebastian Krause, who created a lighthearted work environment. I especially thank Sebastian for the office dinosaurs and GoPro help. I am grateful for Kat Knight, Tiara Moore, and Arik Joukhajian, who assisted in processing samples in the lab and made working long hours a blast.

Finally, I would like to thank my family and my fiancé, Artie, for all of their positive encouragement and genuine interest in my work at UCLA.

This project was funded by USC Sea Grant, in the form of a Graduate Traineeship. A huge thank you goes to the Southern California Marine Institute (SCMI) for allowing us to use their R/V Yellowfin and for their awesome help with the sampling of the sediment cores and operation of the CTD. Heal the Bay at the Santa Monica Pier Aquarium was kind enough to host a summer outreach display of our project.

1 Introduction

1.1 Ocean oxygen minimum zones

Background — Ocean oxygen minimum zones (OMZs) are regions of depleted oxygen concentrations in the subsurface water column. OMZs occur globally and form naturally through a combination of high biological respiration and low supply of O_2 by ocean circulating waters. These areas include: coastal shelf systems, where nutrients are brought up from the subsurface via upwelling; bottom waters of silled basins and fjords, where water exchange is limited; and coastal embayments, where organic matter input is sustained through riverine and terrestrial processes (Middelburg and Levin, 2009; Paulmier and Ruiz-Pino, 2009) (Fig. 1-1). OMZs have gained recent attention due to their areal expansion (Schmidtko et al., 2017; Stramma et al., 2008). According to the fourth assessment report of the Intergovernmental Panel of Climate Change (IPCC), the ocean is substantially warming and becoming more acidic (Kumar, 2007). A warming ocean thereby decreases O_2 solubility and ventilation, resulting in OMZ expansion (Stramma et al., 2008).

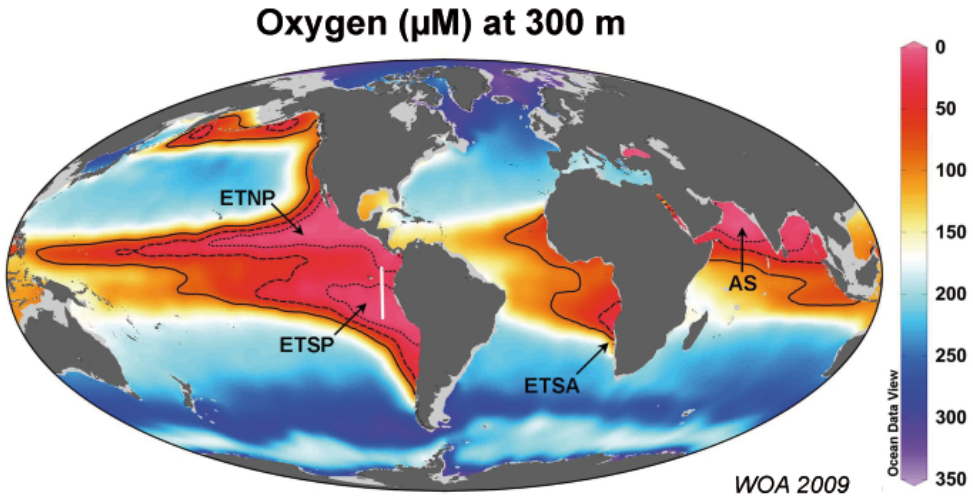

Figure 1-1: **Global oceanic oxygen minimum zones**. Depicted is the oxygen concentration at 300-meter water depth. Image is modified after World Ocean Atlas 2009 (http://www.nodc.noaa.gov)

Negative global consequences — Stramma et al. (2008) used quality-controlled historical data and more recently measured O_2 profiles from 1960 to show that over the past 50 years, Tropical Ocean OMZs have expanded and intensified. Their results supported climate model predictions of declining dissolved O_2 in the tropical pacific and the expansion of the tropical OMZs, due to both thermal stratification constraining the mixing of oxygenated waters and decreasing oxygen solubility from warmer surface waters. By the year 2100, models predict that dissolved O_2 in the global ocean could decline by one to seven percent (Schmidtko et al., 2017). Middelburg and Levin (2009) and Paulmier and Ruiz-Pino (2009) detail several of the negative consequences of the growth of hypoxic and anoxic zones. First, hypoxia has direct and indirect effects on survival, functioning and behavior of many organisms. Second, OMZs are associated with the production of greenhouse gases including oceanic nitrous oxide (N_2O), and methane (CH_4). And lastly, the nitrogen loss associated with OMZs could affect primary production with resulting responses to carbon transport (Wright et al., 2012).

Local effects on marine organisms — Not only are coastal upwelling regions important for nutrient cycling, but a large proportion of the world's fisheries reside in these systems (Stramma et al., 2010). Because hypoxia reduces locomotory functions and metabolic activity in both fishes and squid, many macro-organisms become stressed, migrate away or perish under oxygen concentrations below 120 µM O_2. Additionally, the shoaling, or moving surface-ward, of O_2-depleted waters restricts the depth distribution of large pelagic fishes, making them more vulnerable to surface fishing gear (Prince and Goodyear, 2006). Recent increases in jellyfish populations have been linked to eutrophication and hypoxia because jellyfish and their polyps are more tolerant to hypoxia (Stramma et al., 2010). This could result in a positive OMZ feedback

because jellyfish prey on zooplankton, leaving more phytoplankton free of predation and more available to die, sink and get remineralized, thus adding to the consumption of O_2. Furthermore, most larvae of fish and crustacean species are less tolerant of hypoxia than adults, and a decline in dissolved O_2 could affect their evolution of oxygenation by diffusion to active ventilation of gills (Levin, 2003; Stramma et al., 2010). Gonads also require higher oxygen demands, causing females to out-survive their male counterparts (Pörtner and Farrell, 2008). A decrease in species diversity at the benthic level is associated with OMZs, because specific taxa (i.e. calcareous foraminiferans, nematodes and annelids) are more tolerant of hypoxia compared to less tolerant taxa (i.e. agglutinated protozoans, harpacticoid copepods and calcified invertebrates) (Childress and Seibel, 1998; Levin, 2003). If OMZs continue to expand, genetic diversity and evolution of key species could be strongly influenced (Levin, 2003).

Bioturbation — When there is enough O_2 for macrobenthos to exist, the sediment's solid phase is rearranged by organisms moving around (Jørgensen, 2006; Sturdivant et al., 2012). Bioturbation displaces fresh organic matter, older buried inorganic material (i.e. pyrite and carbonates), other organisms, and reactive nutrients and elements both vertically and horizontally (Kristensen et al., 2012). Evidence of bioturbation can therefore be seen in zigzag geochemical sediment porewater profiles. The lack of bioturbated sediments (laminations) is a good indicator of anoxic (0 µM O_2) and near anoxic (<5 µM O_2) conditions.

Dissolved Oxygen in the Santa Monica Basin — The Santa Monica Basin (SMB) is part of a 14-basin series that make up the California Continental Borderland (Christensen et al., 1994; Gorsline, 1996, 1992) (Fig. 1-2). It is adjacent to the coastline, and reaches 925 m at its deepest point. The SMB is a recipient of high nutrients due to

upwelled subsurface waters and anthropogenic input from the populated Los Angeles coast (Berelson and Stott, 2003; Stramma et al., 2010). Below the SMB's deepest sill depth at 737 m, water is restricted from mixing with surrounding basins, although periodic deep basin flushing events occur every few years, bringing in colder, oxygenated and relatively denser waters (Heintz, 2012; Berelson, 1991). Because of its high nutrient input and isolation from the open ocean, the SMB hosts an OMZ. For the purpose of this study I define hypoxic conditions as sub-surface water containing <60 µM O_2, near-anoxia as <5 µM O_2, and anoxia as undetectable O_2.

Both physical and biological processes control dissolved O_2 in the SMB, including atmospheric exchange, circulation, ventilation, production and respiration (Bograd et al., 2008). The OMZ extends to the central basin's seafloor, where sediment laminations indicate near anoxic conditions. Evidence of the SMB OMZ's expansion over the past few centuries was obtained from box cores in a 1992 lamination study (Christensen et al., 1994; Gorsline, 1992). The study found that macrobenthos inhabited most of the basin floor ~350 years ago; in contrast, a near anoxic area of 1200-1300 km^2 was recorded ~35 years ago, extending outward from the SMB's deepest center of ~ 925 m to 830 m water depth. The present study aims to resolve if the SMB OMZ has expanded, contracted, or stabilized since the 1992 survey of the region.

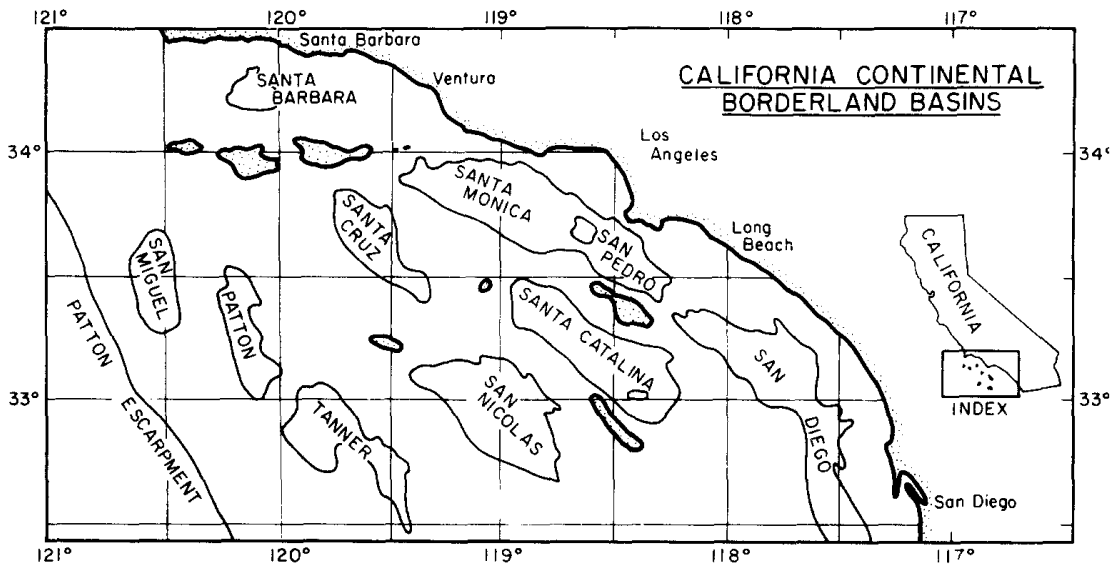

Figure 1-2: California Continental Borderland. Map shows ten basins and Channel Islands. Inner basins are Santa Barbara, Santa Monica, San Pedro and San Diego Trough; central basins are Santa Cruz, Santa Catalina and San Nicolas; outer basins are San Miguel, Patton and Tanner, all from northwest to southeast (modified from Gorsline, 1992).

1.2 Biogeochemical processes in marine sediments

Labile organic matter export to the seafloor provides nutrients and energy for heterotrophic communities in marine sediments (Jørgensen, 2006; Middelburg and Levin, 2009). When particulate organic matter is introduced to the sediment, it is rapidly degraded and mineralized by a broad range of organisms. Microorganisms are the main players in geochemical cycling in marine sediments for four main reasons: their ability to metabolize complex polymeric substances, their capacity to metabolize anaerobically, their small size which enhances their catalytic activity, and their capability to thrive in a wide range of environmental conditions (Jørgensen, 2006; Nealson, 1997). Organic matter degradation by prokaryotes is governed by the availability of electron acceptors following the Gibbs free energy gain sequence (Fig. 1-3). In organic-rich sediments underlying oxygenated waters, O_2 is used up rapidly in the first few millimeters of the sediment because of its highest energy gain and versatile

substrate utilization (Jørgensen, 2000). In deep-sea sediments, less organic matter reaches the seafloor because more of it gets degraded throughout the water column. In these regions, O_2 penetration depths can reach meters into the sediment (Wenzhöfer and Glud, 2002). In the sediment, once O_2 is depleted, consumers degrade organic matter using nitrate, manganese (IV), iron (III), sulfate and carbon dioxide, in that order (Fig. 1-3).

Porewater chemistry

Pathways	Concentration	Stoichiometry	ΔG^0 (kJ mol^{-1})
Oxic/aerobic respiration	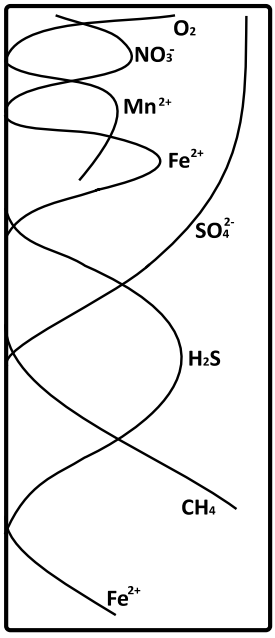	$[CH_2O] + O_2 \rightarrow CO_2 + H_2O$	-479
Denitrification		$5[CH_2O] + 4NO_3^- \rightarrow 2N_2 + 4HCO_3^- + CO_2 + 3H_2O$	-453
Manganese reduction		$[CH_2O] + 3CO_2 + H_2O + 2MnO_2 \rightarrow 2Mn^{2+} + 4HCO_3$	-349
Iron reduction		$[CH_2O] + 7CO_2 + 4Fe(OH)^3 \rightarrow 4Fe^{2+} + 8HCO_3 + 3H_2O$	-114
Sulfate reduction		$2[CH_2O] + SO_4^{2-} \rightarrow H_2S + 2HCO_3^-$	-77
		$4H_2 + SO_4^{2-} + H^+ \rightarrow HS^- + 4H_2O$	-152
		$CH_3COO^- + SO_4^{2-} + 2H^+ \rightarrow 2CO_2 + HS^- + 2H_2O$	-41
Methanogenesis		$4H_2 + HCO_3^- + H^+ \rightarrow CH_4 + 3H_2O$	-136
		$CH_3COO^- + H^+ \rightarrow CH_4 + CO_2$	-28

Figure 1-3: Porewater chemistry. Biogeochemical zonation of organic matter degradation in marine sediments, modified from Jørgensen & Kasten (2006). Left: Mineralization pathways and porewater concentrations of the related dissolved species, Right: Stoichiometry and Gibbs free energy (ΔG0) for each pathway, after Jørgensen & Kasten (2006).

Iron is the fourth most abundant element in the continental crust (Jørgensen, 2006). Iron enters the ocean system and is transported to marine sediments through glacial, aeolian, fluvial and hydrothermal input. It occurs in two valence states, oxidized iron (Fe (III)) and reduced iron (Fe (II)), and is used for either cell growth or to maintain metabolic activity. The accumulation of dissolved Fe (II) can be detected in

sediment porewater. Moreover, it is important to evaluate Fe (II) and phosphate (PO_4^{3-}) together in the porewater since the same processes control both of them. In order to make organic matter more degradable, microbes use phosphatases to remove PO_4^{3-} from organic matter (Kraal et al., 2012). Solid iron oxides scavenge the dissolved PO_4^{3-} produced and when iron is reduced, the PO_4^{3-} is released (Jørgensen, 2006). Therefore, Fe (II) and PO_4^{3-} profiles in the sediment pore water often show similar distributions. Iron, an essential micronutrient for phytoplankton, is incorporated into respiratory pigments, proteins and enzymes, and phosphorous is necessary for basic biomass formation. If there is oxygen in the water column, reduced iron will oxidize to Fe (III). Fe (III) has a high affinity for anions, like PO_4^{3-}, and therefore the PO_4^{3-} will also get 'trapped' by Fe (III) in solid phase, preventing PO_4^{3-}, and thus Fe (II), from reaching shallower water depths. In near anoxic to anoxic bottom water environments, Fe (II) and PO_4^{3-} can diffuse upwards through the sediment and escape into the water column, creating a positive feedback to the OMZ's expansion/stabilization.

Sulfate (SO_4^{2-}) is the most common anion in the ocean after chloride and is transported to the ocean in the form of sulfur, which is present in fluvial input of continental rock fragments (Jørgensen, 2006). Because SO_4^{2-} is so abundant in the marine system, microbial SO_4^{2-} reduction is a dominant way to degrade organic matter in anoxic sediments. As the amount of organic matter increases, the importance of SO_4^{2-} reduction also increases. The product of dissimilatory SO_4^{2-} reduction, hydrogen sulfide (H_2S), collects in the sediment porewater and can either be used as an energy source by sulfur-oxidizing bacteria or react with Fe (II) to form black iron sulfide minerals, a visual indicator for reduced conditions in the sediment.

With increasing organic matter degradation, ammonium (NH_4^+) concentration and total alkalinity (TA) both accrue in the sediment porewater. NH_4^+ is produced

through ammonification of organic matter, and TA is set by the net charge contribution from collected conservative anions (Cl^-, So_4^{2-}, Br^-, and F^-), conservative cations (NA^+, Mg^{2+}, Ca^{2+}, K^+, Sr^{2+}), non-conservative anions (HCO_3^-, CO_3^{2-}, $B(OH)_4^-$ and OH^-) and non-conservative cations (H^+) (Williams and Follows, 2011). During sulfate reduction, bicarbonate (HCO_3^-) is produced, increasing TA. Geochemical profiles of increasing NH_4^+ and TA with depth are a good indication of anaerobic bacterial degradation. In this study, sediment cores were used to analyze supernatant water and porewater for dissolved iron (Fe (II)), phosphate (PO_4^{3-}), total sulfide (sulfide), ammonium (NH_4^+), total alkalinity (TA), sulfate (SO_4^{2-}), and sulfate reduction rates.

1.3 Aim of this work

The main objective of this study is to provide geochemical and biologic information on the benthic environment in the SMB since the last survey, reported in Gorsline (1992). We provide insight into the processes related to sub-oxic conditions in the water column and how this might contribute to the SMB OMZ's stabilization, expansion or reduction. Four hypotheses can be generated about SMB OMZ sediments:

1. **The anoxic/hypoxic zone of the SMB is characterized by iron and phosphorous releases from the seafloor into the water column,**
2. **Bacterial sulfate reduction is enhanced in sediments underlying anoxic/hypoxic bottom water,**
3. **Bioturbation is absent from sediment cores underlying anoxic/hypoxic bottom water, and**

4. **All three of these factors are present in sediment cores retrieved at depths shallower than 830 m, indicating that the OMZ in the Santa Monica Basin has expanded since the last survey of the area in 1992.**

2 Materials and methods

2.1 Study site

Geographical setting — Around 30 million years ago, the North America plate overrode the East Pacific Mid-Ocean Ridge and caused large-scale lateral shearing motions on the North American plate's edge (Gorsline, 1992). Through rifting, a series of active margin basins were formed, including the inner Santa Monica and San Pedro Basins, both the closest of all basins to the Los Angeles coast and part of a 14 basin set that forms the Southern California Bight (Christensen et al., 1994; Gorsline, 1996, 1992). The modern Santa Monica Basin (SMB) is approximately 40 km wide by 100 km long with a maximum depth of 925 m. Below its deepest sill at 737 m, the basin is defined as closed. Between 700 and 737 m, connections with the San Pedro Basin, the San Diego Trough and the Santa Catalina Basin start to widen and at 600 m, the connection between the SMB and the Santa Catalina Basin opens. At water depths less than 250 m, the surface waters of all of the neighboring basins, except the Santa Barbara Basin, are connected (Heintz et al., 2012). Mixing with deep oxygenated water from adjacent basins is limited because of the surrounding topographic ridges making up the southern California Borderland (Berelson, 1991). Compressional forces over the past 4 to 5 million years have caused downward displacement of the basins, which have been filling with terrigenous and biogenous sedimentary material (Gorsline, 1992).

Physical oceanography — The oceanography of the Southern California Bight is dominated by the California Current system, an eastern boundary current system comprised of north and southward-flowing currents (Jackson, 1992). Offshore of the California Bight, the California Current brings cold subarctic water equatorward. Shoreward of the California Current, the Southern California Countercurrent

transports warm, high salinity water from the equatorial Pacific. However, equatorward winds along the coast of Southern California cause Ekman transport of surface waters away from the coast and upwelling of cooler, subsurface water (Huyer, 1983). Places of coastal upwelling are highly productive because of the transport of nutrients to the euphotic zone leading to extensive phytoplankton blooms (Chavez and Messié, 2009; Gruber et al., 2011; Huyer, 1983).

Sedimentation — The term sediment is used here to describe material with terrigenous, biogenous and/or anthropogenic sources. Because the SMB is adjacent to a coastline, it serves as a natural sediment trap (Huh et al., 1990; Berelson, 1991). During the past 10,000 years, 10-12 m of sediment has entered the basin via several processes: particle infall, nepheloid plumes, turbidity currents, and mass movements (Gorsline, 1992). Particle infall refers to biologically formed aggregates created through biological blooms, nutrient runoff from the mainland, and aeolian input. Bacteria degradation and benthic organism re-working of biologically composed sediment masks the true sedimentation of bioaggregates. Nepheloid flows, clouds of suspended particles in the water column, move along isopycnals adjacent to the ocean floor and are formed primarily by terrigenous sources (Gorsline, 1992; Plank and Zaneveld, 1972). Both turbidity currents and mass movements, triggered by seismic shocks, are infrequent on centennial time scales. Storm waves and floods also trigger turbidity currents.

Since the beginning of this century, the dramatic increase in human population of the Los Angeles region has introduced immense drainage of human and industrial by-products into the ocean (Berelson, 1991; Dojiri et al., 2003). Based on sediment budget calculations, Alexander et al. (2003) estimated that 50-100% of the natural and anthropogenic inputs are retained in the SMB (Alexander and Venherm, 2003). These

inputs include contaminants from: wastewater treatment facilities, storm water runoff, atmospheric fallout and marine-related activities.

Oxygen in the Santa Monica Basin — Dissolved O_2 in the SMB is controlled by both physical and biologic processes including atmospheric exchange, circulation, ventilation, photosynthesis and respiration (Bograd et al., 2008). Introduction of nutrient-rich water at the surface stimulates phytoplankton blooms; photosynthesis increases surface O_2 while respiration of the sinking bloom at depth consumes O_2, creating the SMB OMZ. Below the SMB sill depth, water is restricted from mixing with surrounding basins.

Around 350 years ago, most of the SMB was inhabited by macrobenthos, seen in bioturbated box core sediments (Fig 2-1) (Gorsline, 1992). Between 350-300 years ago, a small, very low oxygen content bottom water area of 120 km^2 formed and from 300-23 years ago, the near-anoxic (<5 µM dissolved O_2) area of 1200-1300 km^2 spread to the basin floor below water depths of about 830 m (Christensen et al., 1994; Gorsline, 1992). Using hydrographic data from 1984-2006, Bograd et al. (2008) found that within portions of the California Current System, the hypoxic boundary (~60 µM O_2) had shoaled up to 90 m below sea surface due to decreased vertical mixing of oxygenated water from surface warming causing enhanced stratification (Bograd et al., 2008). In order to evaluate the behavior of the OMZ since 1992 to present, the spatial scheme adapted from Gorsline (1992) was used as the baseline for sample collection (Christensen et al., 1994; Gorsline, 1992).

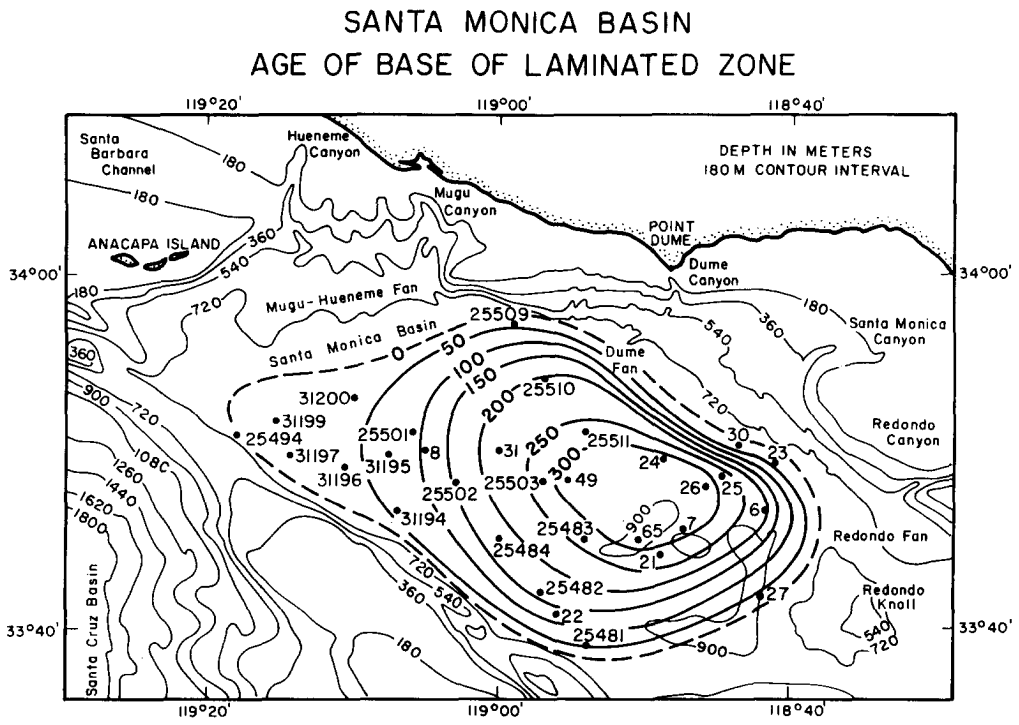

Figure 2-1: SMB lamination zone. Isopleths of the age (years before present (BP)) of the base of the nonbioturbated laminated sediments in the Santa Monica Basin. The maximum core thickness of the central oldest area is about 17 cm at in situ bulk densities. Reprinted from Gorsline, 1992.

2.2 Water column and sediment sampling

Sampling transects — Cores were collected along two transects, both transitioning from outside to inside the 1992 OMZ. The term MUC refers to stations where a sediment multicorer was deployed. Transect 1 contained nine MUC stations spanning between 71 and 907 m water depth, from the oxygenated coastal shelf to the most oxygen-deplete region at the deepest part of the basin near its center (71, 154, 319, 399, 485, 537, 695, 777 and 907 m; Fig. 2-2). Transect 2 comprised three MUC stations located perpendicular to Transect 1 from shallow to deep (508, 745 and 893 m). Before sediment cores were taken at all stations, dissolved O_2 concentrations in the water column of the SMB were obtained at five stations along Transect 1 (154, 399, 537, 777, and 907 m water depth) using a conductivity, temperature and density

instrument (CTD, Sea-Bird 25) with attached Seapoint chlorophyll flourometer, SBE43 oxygen sensor (Winkler titration), and a QSP200PD biospherical photosynthetically active radiation (PAR) sensor. For calibration, automated bath systems, sensor stability, primary standards in temperature (water triple point and gallium melting point) and conductivity (International Association for the Physical Sciences of the Oceans: IAPSO) are maintained. Sediment cores were retrieved at these same five stations during later field days and used as part of the 12 MUCs (CTD 1=MUC 5, CTD 2=MUC 3, CTD 3=MUC 7, CTD 4=MUC 2, CTD 5=MUC 1). For simplicity, I will refer to the CTD and MUC stations by their water depth (m). Core ID, location, and water depth from all 12 MUCs and bottom water temperature and dissolved O_2 concentrations from the 5 CTD stations are shown in Table 1.

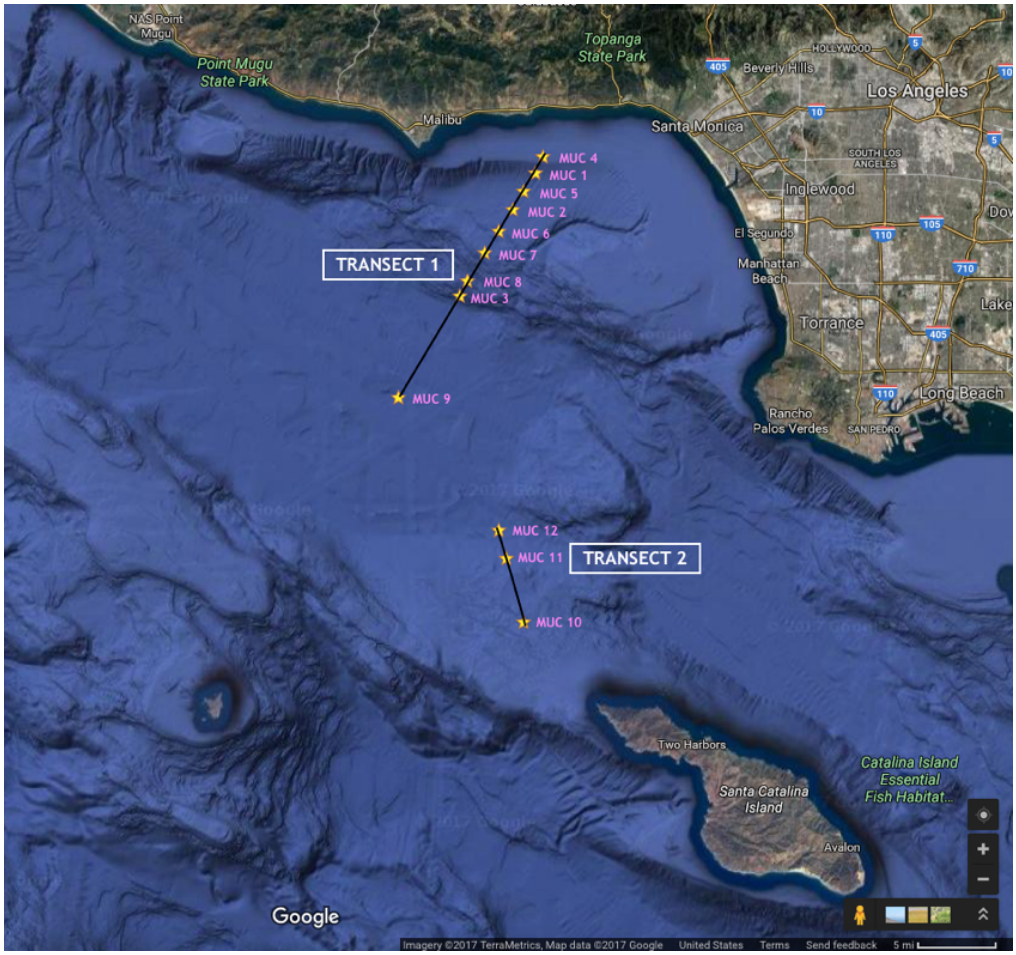

Figure 2-2: **MUC station transects**. (Map Data: Google Earth, 2017)

Table 2-1: SMB sampling deployment information. Bottom water temperature (˚C) and bottom water O_2 concentration (µM) measured by CTD at five of the 12 stations. Note that CTD measurements were obtained on May 24, 2016.

Station	Core ID	Date (2016)	Latitude (N)	Longitude (W)	Depth (m)	Bottom Water Temp. (˚C)	Bottom Water O_2 (µM)
1 (*CTD 5*)	MUC 1	May 26 (*May 24*)	33˚58.545'	118˚40.460'	154	9.4	61.1
2 (*CTD 4*)	MUC 2	May 26 (*May 24*)	33˚56.483'	118˚42.007'	399	7.8	31.7
3 (*CTD 2*)	MUC 3	May 26 (*May 24*)	33˚51.669'	118˚45.615'	777	5.2	5.6
4	MUC 4	July 13	33˚59.435'	118˚39.966'	71		
5	MUC 5	July 13	33˚57.549'	118˚41.294'	319		
6	MUC 6	July 13	33˚55.259'	118˚42.925'	485		
7 (*CTD 3*)	MUC 7	July 21 (*May 24*)	33˚54.070'	118˚43.911'	537	6.7	14.5
8	MUC 8	July 21 (*May 24*)	33˚52.503'	118˚45.107'	695		
9 (*CTD 1*)	MUC 9	July 21	33˚46.880'	118˚49.164'	907	5.1	4.4
10	MUC 10	July 27	33˚38.495'	118˚42.939'	893		
11	MUC 11	July 27	33˚36.907'	118˚42.477'	745		
12	MUC 12	July 27	33˚33.298'	118˚41.296'	508		

Sampling — Samples were retrieved using a sediment multicorer equipped with 4 polycarbonate core liners (Fig. 2-3). The liners were 60 cm long with an inner diameter of 9.5 cm. After collection, sediment cores were immediately capped with a rubber stopper on each end. Cores were selected for porewater analyses, solid phase analyses, sulfate reduction, macrofauna identification and ^{210}Pb geochronology analyses (Table 2-2). Cores for macrofauna and ^{210}Pb dating were transported to the University Southern California for further processing (laboratory of Prof. William Berelson) and were not part of this thesis project.

Cores for porewater analyses, solid phase analyses, and sulfate reduction were wrapped with ice-sheets and insulation blankets (aluminum), and transported carefully upright from the San Pedro harbor to a 4˚C cold room at UCLA where they were further processed. To mitigate potential O_2 contamination, cores from the first three MUC

stations (154, 399, and 777 m) were sliced and analyzed for porewater measurements within 24 hours after retrieval. However, O_2 concentrations in the supernatant water of replicate MUC 1-3 cores measured by point optodes (PreSens) over 15 days in the cold room (stored in the dark) showed no critical decline in O_2, although some O_2 may have been introduced when the cores were extracted from the multicorer (Fig. 2-4). Therefore, MUCs 4-12 were stored overnight in the cold room before slicing and analyses. O_2 concentrations in the cores were measured using a handheld Microx 4 trace fiber optic oxygen meter (PreSens) and Oxygen Sensor Spots SP-PSt7-NAU (PreSens; standard measurement range of 0-100% O_2 and detection limit of 0.03% O_2). Although we trust the trend of our PreSens optode measurements of O_2 in supernatant waters from the individual cores (Fig. 2-4), we do not trust the absolute measurements after comparing with CTD data. It was possible that O_2 diffusion occurred as a result of contact with air during the capping of cores on board.

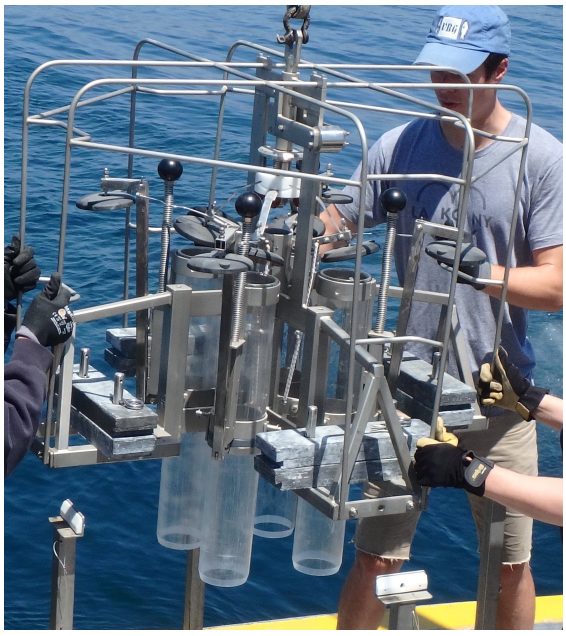

Figure 2-3: **Sediment multicorer.** The MUC had 4 polycarbonate core liners of 60 cm length and 9.5 cm inner diameter.

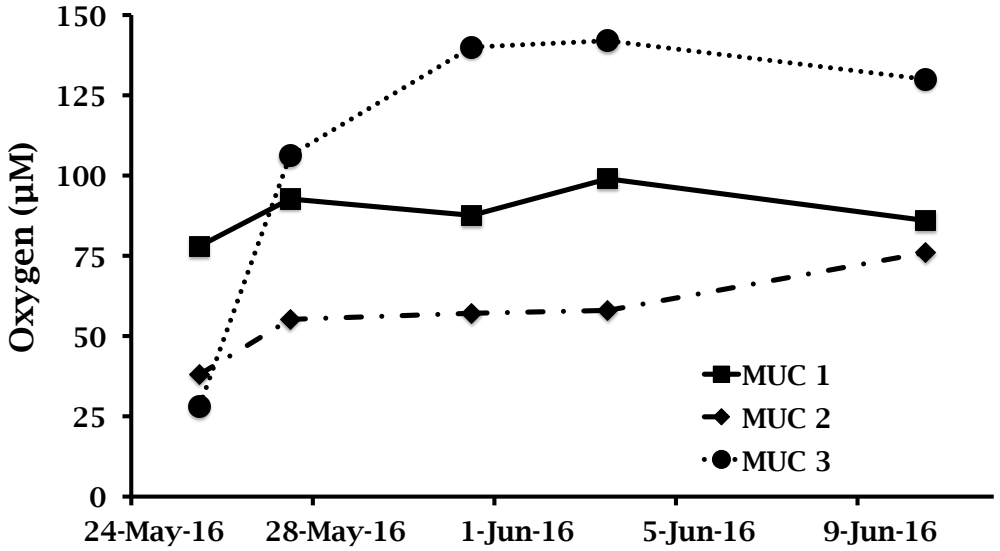

Figure 2-4: **Optode readings for MUCs 1-3.** The first reading was taken on May 25, 2016 after the cores were taken off the multicorer and capped aboard the R/V Yellowfin. The subsequent readings were taken in the cold room at UCLA. Although the trends show diffusion of oxygen into the sediment after being capped, they do not show substantial O_2 decline during storage.

Table 2-2: **Core selections.** Core ID and assigned analyses for the 4 cores obtained from each MUC sampling. Note that Dr. William Berelson's group at University of Southern California performed both the macrofauna analysis and Cs-137 and PB-210 dating.

Core ID	Core Selections
MUC 1	1 core for porewater, 1 for solid phase, 1 for sulfate reduction, 1 for macrofauna (USC).
MUC 2	1 core for porewater, 1 for solid phase, 1 for sulfate reduction, 1 for macrofauna (USC).
MUC 3	1 core for porewater, 1 for solid phase, 1 for sulfate reduction, 1 for macrofauna (USC).
MUC 4	1 core for porewater, 1 for solid phase and sulfate reduction (combined), 1 for macrofauna (USC), 1 for dating (USC).
MUC 5	1 core for porewater, 1 for solid phase and sulfate reduction (combined), 1 for macrofauna (USC), 1 for dating (USC). Optode core.
MUC 6	1 core for porewater, 1 for solid phase and sulfate reduction (combined), 1 for macrofauna (USC), 1 for dating (USC). Used sediment from 20-24 cm for methanogenesis experiment.
MUC 7	1 core for porewater, 1 for solid phase and sulfate reduction (combined), 1 for macrofauna (USC), 1 for dating (USC). Optode core.
MUC 8	1 core for porewater, 1 for solid phase and sulfate reduction (combined), 1 for macrofauna (USC), 1 for dating (USC).
MUC 9	1 core for porewater, 1 for solid phase and sulfate reduction (combined), 1 for macrofauna (USC), 1 for dating (USC).
MUC 10	1 core for porewater, 1 for solid phase and sulfate reduction (combined), 1 for macrofauna (USC), 1 for dating (USC). Optode core.
MUC 11	1 core for porewater, 1 for solid phase and sulfate reduction (combined), 1 for macrofauna (USC), 1 for dating (USC). Optode core.
MUC 12	1 core for porewater, 1 for solid phase and sulfate reduction (combined), 1 for macrofauna (USC), 1 for dating (USC). Surface of core was uneven (probably MUC penetration not vertical). Optode core.

2.3 Porewater analyses

Geochemical Analyses — From each of the 12 MUC stations, one core was sliced in the cold room (4˚C) for porewater analyses. Before slicing, a 50 mL subsample of the supernatant was suctioned into an argon-flushed 60 mL syringe and transferred to an argon flushed 50 mL centrifuge tube. Before closing the lid of the tube, the headspace was flushed again with argon. After the supernatant was sub-sampled the remainder of the water was discarded. The core sediment was sliced at 1-cm intervals from 0-10 cm, 2-cm intervals from 10-20 cm, and 4-cm intervals from 20-32 cm. During each slicing step, the top sediment layer was subjected to a constant argon flow to minimize contact with oxygen. From each sampled slice, approximately 45 cm^3 of sediment was transferred to duplicate argon-flushed 50 mL centrifuge tubes and the headspace of the tube was flushed with argon before the lid was closed.

After centrifugation (3400 g, 20 minutes, 68˚C), the porewater was split as follows (Fig. 2-4): From tube 1, 1 mL was pipetted into separate 6-mL plastic scintillation vials for ferrous iron (Fe (II)), ammonium (NH_4^+), and total sulfide measurements; 2 mL were pipetted into a 6-mL scintillation vial for orthophosphate (PO_4^{3-}) determination. From tube 2, 1 mL of porewater was added to 2-mL cryovials for sulfate (SO_4^{2-}) and nitrate (NO_3^-) determinations and stored at 80˚C. The remaining porewater of both centrifuge tubes was then combined in 20-mL plastic scintillation vials. From this combined porewater, 0.5 mL was pipetted into titration vials for total alkalinity (TA) measurements.

Concentrations of Fe (II), sulfide, NH_4^+, and PO_4^{3-} were measured on a Shimadzu UV-1800 UV spectrophotometer using standard photometric procedures (Grasshoff, Kremlingl, et al., 1999). Sulfide and Fe (II) are very sensitive to O_2 and therefore extra precautions were put in place to avoid O_2 contamination during addition of reagents.

First, standards for both Fe (II) and sulfide were prepared in an anoxic glove bag. Before porewater or reagents were added to the empty scintillation vials, the vials were flushed with argon for 10 seconds each. Additionally, the reagent bottle headspaces and pipettes were flushed with argon during the addition of the reagents to the samples.

For Fe (II) analyses, the stock standard solution was created by dissolving 4.9765 g (17.9 mmol) of fresh $FeS0_4*7H_20$ (lron (II)-sulfate-hepta-hydrate) and 3.154 g (17.9 mmol) of ascorbic acid in exactly 100 ml of pure 0_2-free MilliQ water. The work standard was created by adding 1.0 mL of the stock solution to 0.5 mL of 1% ascorbic acid and filling to 100 mL exactly with pure 0_2-free MilliQ water. Fe (II) forms a violet colored complex with Ferrospectral. After l mL of the porewater sample was pipetted into the argon pre-flushed scintillation vial, 10 µL of a 1% of the ascorbic acid solution, 4 mL of O_2-free seawater and 50 µL of the Ferrospectral color reagent (Merck #111613; VWR #AAAL10607-06) were added, in that order. The sample was mixed and after 10 minutes, the violet colored complex was quantified at a wavelength of 565 nm.

Hydrogen sulfide stock and work standards were also made in an anoxic glove bag. For the stock standard, 75 mg of $Na_2S * 9 H_2O$ (Millipore Sigma, *sodium sulfide hydrate; CAS#27610-45-3*) was dissolved in 100 mL O_2-free seawater (concentration: 3.125 mM S^{2-}). For the work standard, 25 mL of the stock solution was poured into a graduated cylinder, 25 mL of the zinc acetate gelatin solution was added and, if necessary, the solution was made up to a total of 50 mL with O_2-free seawater (conc.: 1561.3 µM S^{2-}). 50 µL of the zinc acetate gelatin solution was pipetted into an argon pre-flushed 6 mL scintillation vial. Next, 1 mL of the sample was added. 10 µL of both the color reagent and the catalyst were added, and the samples were measured after 1 hour. To avoid losses of H_2S the zinc acetate gelatin solution had to be added

immediately after sampling. Sulfide was determined as methylene blue, formed from dimethyl-p-phenylenediamine by hydrogen sulfide in an acidic medium using the reaction with Fe (III) chloride as an oxidant; measured at 670 nm.

NH_4^+ was measured as indophenol blue, formed by phenol and hypochlorite in the presence of NH_3. Nitroprusside was used as the catalyst in the reaction and dichloro-s-triazine-2,4,6-(1H,3H,5H)-trione sodium salt (DTT) was used as an alternative hypochlorite donor. 5 mL of seawater samples and 1 mL of porewater sample plus 4 mL MilliQ water were used. After the sample was added, 200 mL of the phenol/nitroprusside solution was pipetted into to the vial. After 2 minutes 100 mL of the citrate buffer and 200 mL of the DTT reagent was added, vials were mixed and kept in aluminum foil for 10-18 hours until measured at 630 nm. Standards were made using Millipore Sigma Ammonium Standard Solution Trace (EMD 1.19812.0500).

Phosphate (PO_4^{3-}) was determined by the reaction of the PO_4^{3-} ions with an acidified molybdate reagent to yield a phosphomolybdate heteropoly acid, which was then reduced to a blue compound, and measured at 880 nm after 10 minutes. After 2 mL of pore water sample or standard were made up to 5 mL with pure water, 0.1 mL of the ascorbic acid solution and 0.1 mL of the heptamolybdate reagent were added. Analysis of seawater samples did not require any dilution. The PO_4^{3-} stock standard was made by diluting a PO_4^{-3}-standard (MERCK Titrisol ™, Millipore EMD 1.09870.0001) with pure MilliQ water to exactly 1 L. The stock solution was diluted to make the work standards.

NO_3^- and SO_4^{2-} concentrations were determined by ion chromatography (Metrohm 930 Compact IC Flex) with a conventional anion exchange column (MetroSep Supp 5-250/40) using an eluent solution of sodium carbonate (3.2 mM) and bicarbonate (1.0 mM) and a regenerator solution of sulfuric acid (500 mM) with oxalic

acid (100 mM). Samples for ion chromatography were pre-filtered through a 0.2 µm AcroDisk filter, IAPSO Standard Seawater was used for SO_4^{2-} calibration, and a EMB Millipore Corporation nitrate standard solution, certified reference material (CRM) traceable to standard reference material (SRM) from the National Institute of Standards and Technology (NIST) 2.50 mg/l NO^{3-} N in H_2O was used for NO_3^- calibration. TA was measured by titrating 500 µL of subsample with 0.01 M HCl Titrisol solution (Merck) using a methyl red and methyl blue indicator solution and an electronic burette (876 Dosimat plus Metrohm) (TA, Ivanenkov and Lyakhin 1978). For the calibration of TA, IAPSO Standard Seawater was first titrated three times.

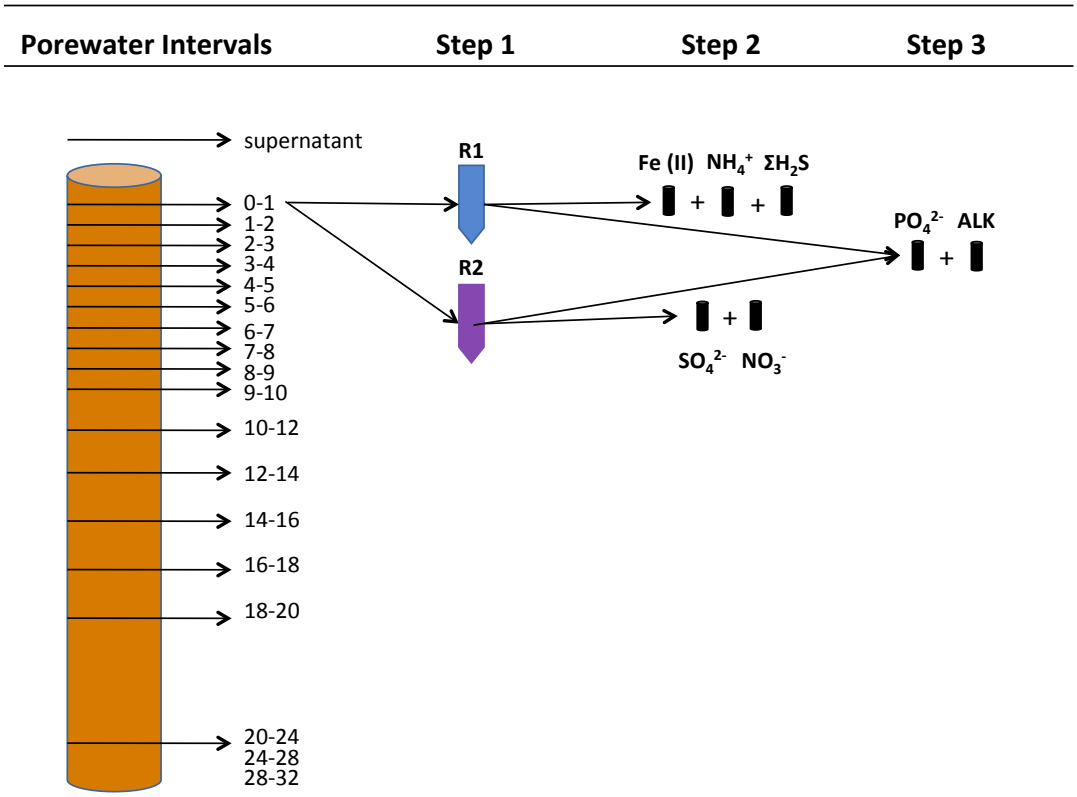

Figure 2-5: Destination of porewater samples. Schematic of the sediment-slicing procedure for porewater extraction. For details, see text. R1, R2 = replicate centrifuge tubes.

2.4 Sulfate reduction

Sulfate reduction was determined using the whole-round core radiotracer

injection method by (Jørgensen, 1978). A single push core (length 30 cm, inner diameter 2.6 cm) was subsampled from the selected MUC core. For MUCS 1-3 (154, 399 and 777 m, respectively) two replicate push cores were subsampled. Next, 6 µL of the carrier-free $^{35}SO_4^{2-}$ radiotracer (specific activity 37 TBq mmol^{-1}, 200 kBq for MUC 1-3 and 300 kBq for MUC 4-12, dissolved in water; American Radiolabeled Chemicals Inc.) was injected into the push cores at 1-cm depth intervals. The push cores were incubated at 7˚C in the dark for ca. 16 hours. After the incubations, bacterial activity was terminated by slicing the cores into 1-cm intervals and transferring the sediment into 50 mL centrifuge tubes filled with 20 mL zinc acetate (20 % w/w). Control sediment was terminated before radiotracer addition. After transfer to zinc acetate, samples stored at -20˚C to prevent re-oxidation of ^{35}S-sulfides (Røy et al., 2014). Sulfate reduction rates were determined using the cold-chromium distillation method according to (Kallmeyer et al., 2004). For porosity measurements, sediment samples were weighed wet and dry and corrected for salt content.

3 Results

3.1 Sediment descriptions

Core descriptions and porewater analyses are presented in order of shallowest to deepest water depth, separately for Transect 1 (MUCs 1-9) and Transect 2 (MUCs 10-12). Average porosity data for each MUC is shown in Table 1, and all porosity data is presented in the Appendix (Table 5-5). All MUCs exhibited the highest porosity at the top of the core with decreasing porosity downcore. Overall, the average porosity for each station increased with increasing water depth, with the exception of the station at 537 m (MUC 7) (Table 1). Photos of each core used for porewater measurements are presented in Fig. 1.

From Transect 1, both the stations at 71 m (MUC 4) and at 154 m (MUC 1) were a mixture of sand and clay (average porosity of 0.57 and 0.58, respectively). These shallow cores exhibited olive-green/grey colors (Fig. 1). The 71 m station's sediment contained worm burrows with small worms visible and the 154 m station's sediment contained burrows between 8-15 cm. The station at 319 m (MUC 5) had an average porosity of 0.7 and small worm tubes (ca. 1 mm diameter) were seen sticking out of the muddy sediment. At 399 m (MUC 2), the sediment was silty (average porosity of 0.68), burrows were present at 5-8 cm and a blackish ring occurred at 8-15 cm. Small, white sand-sized particles (potentially foraminifera) were seen at 485 m (MUC 6) between 0-13 cm and tiny worm tubes (ca. 1 mm diameter) were sticking out of muddy sediment at around 2 to 3 cm down the core. At 537 m (MUC 7), the sediment was muddy (average porosity of 0.7) and both shrimp (ca. 1 cm) and burrows were visible at 8 cm. At 695 m (MUC 8), the muddy sediment contained worm tubes sticking out of surface, burrows at 10-15 cm and silicate sponge spicules from 10-30 cm. The sediment at 777 m (MUC 3) was olive green with some reddish parts; worm tubes stuck out of surface

and possible burrows were visible at 18-25 cm. The core was muddy with a very 'fluffy' core top (porosity at 0.5 cm was 0.9 and at 19 cm was 0.77; Appendix, Table 5-5). There were no animals present at the deepest station at 907 m (MUC 9) (average porosity of 0.84). This station's sediment was very soft and fluffy, particularly at the surface; from 0-2 cm, the core had a high porosity of ~ 0.9. A light brown lamina was seen from 0-2 cm, followed by darker brown and white lamina from 2-5 cm. From 5-11 cm, the sediment was reddish brown, with some darker brown lamina until 17 cm. The core was olive green from 17-30 cm, and grey from 30-40 cm.

From Transect 2, the sediment at 508 m (MUC 12) was olive-green; with white dots at 0-4 cm and one worm tube (ca. 3-4 mm diameter) was sticking out of the sediment. At 745 m (MUC 11) the core was also olive-green with burrows at 0-10 cm and a large (4-5 cm) errant polychaete was visible on top of the sediment. No animals were present at the deepest station from Transect 2 at 893 m (MUC 10). The average porosity of MUC 10 was 0.82. The core was muddy, red/brownish from 0-1 cm, olive-green from 1-18 cm, and grey from 18-33 cm with an average porosity of 0.82.

No large, filamentous sulfur bacteria were seen on top of or inside any sediment cores at any station. No animals were reported at the two deepest stations only.

Table 3-1: Average porosity. Average porosity data for each MUC station, in order of water depth from shallow to deep.

MUC ID	Water depth (m)	Average Porosity	Depth of Average Porosity (cm)
4	71	0.570	8
1	154	0.583	5
5	319	0.697	14
2	399	0.680	19
6	485	0.747	26
7	537	0.689	22
8	695	0.787	30
3	777	0.810	19
9	907	0.839	32
*12	508	0.698	22
*11	745	0.834	28
*10	893	0.817	30

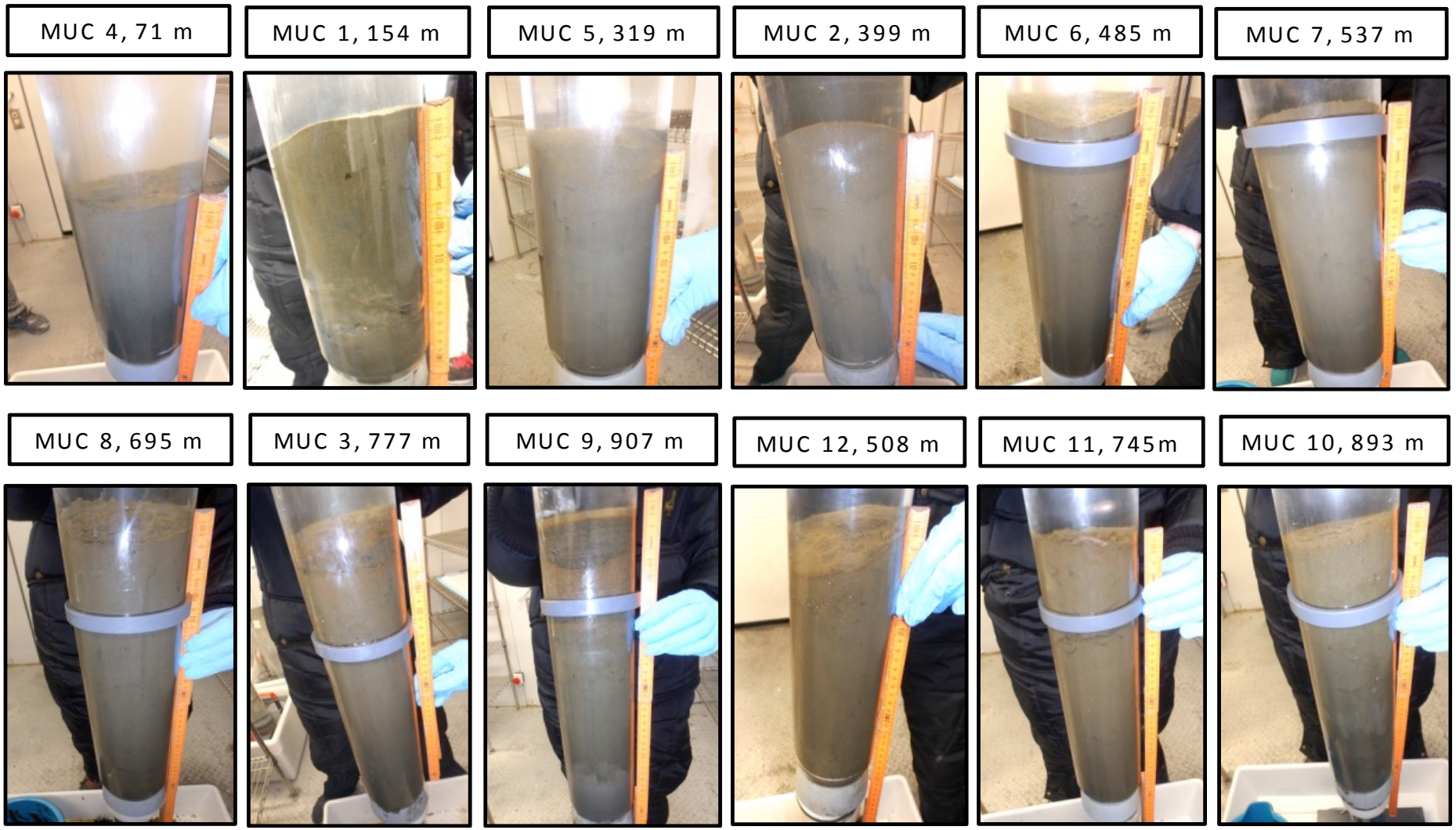

Figure 3-1: MUC sediment core photographs. Images of each MUC core used for porewater analyses, taken minutes before slicing the cores in the cold room. Signs of clear bioturbation were seen in MUC 1, laminations were visible in MUC 9, and a polychaete was seen on the core surface in MUC 11.

3.2 Water column data

Water column profiles of dissolved oxygen (O_2), temperature, and fluorescence are presented for increasing depths of 154, 319, 399, 777, and 907 m (MUCs 1, 2, 7, 3, and 9, respectively) in Fig. 2. These data were collected by CTD casts before any sediment was collected. For stations at 154, 319, 399, 777, and 907 m, dissolved O_2 surface concentrations were 243, 225, 247, 242, and 244 µM, respectively and dissolved O_2 bottom water concentrations were 61, 32, 15, 5.6 and 4.4 µM, respectively (Fig. 3-2). For stations at 154, 319 and 399 m, dissolved O_2 minima occurred at the bottom depths. For stations at 777 and 907 m, dissolved O_2 minima occurred ~705 m (4.3 and 3.4 µM, respectively). From shallowest to deepest CTD cast, temperature maxima (17.7, 18, 17.9, 15.8 and 15.9˚C, respectively) occurred at the surface for each station and minima (5.1, 5.2, 6.7, 7.8 and 9.4˚C, respectively) occurred at the bottom depth. Fluorescence was 0 mg/L from the surface to 59 m below sea level at 154 m (MUC 1), probably due to a malfunctioning instrument sensor. At 319, 399, 777, and 907 m, fluorescence maxima occurred between 10 and 50 m below sea level (2.7, 1.5, 3.0 and 3.1 mg/L, respectively).

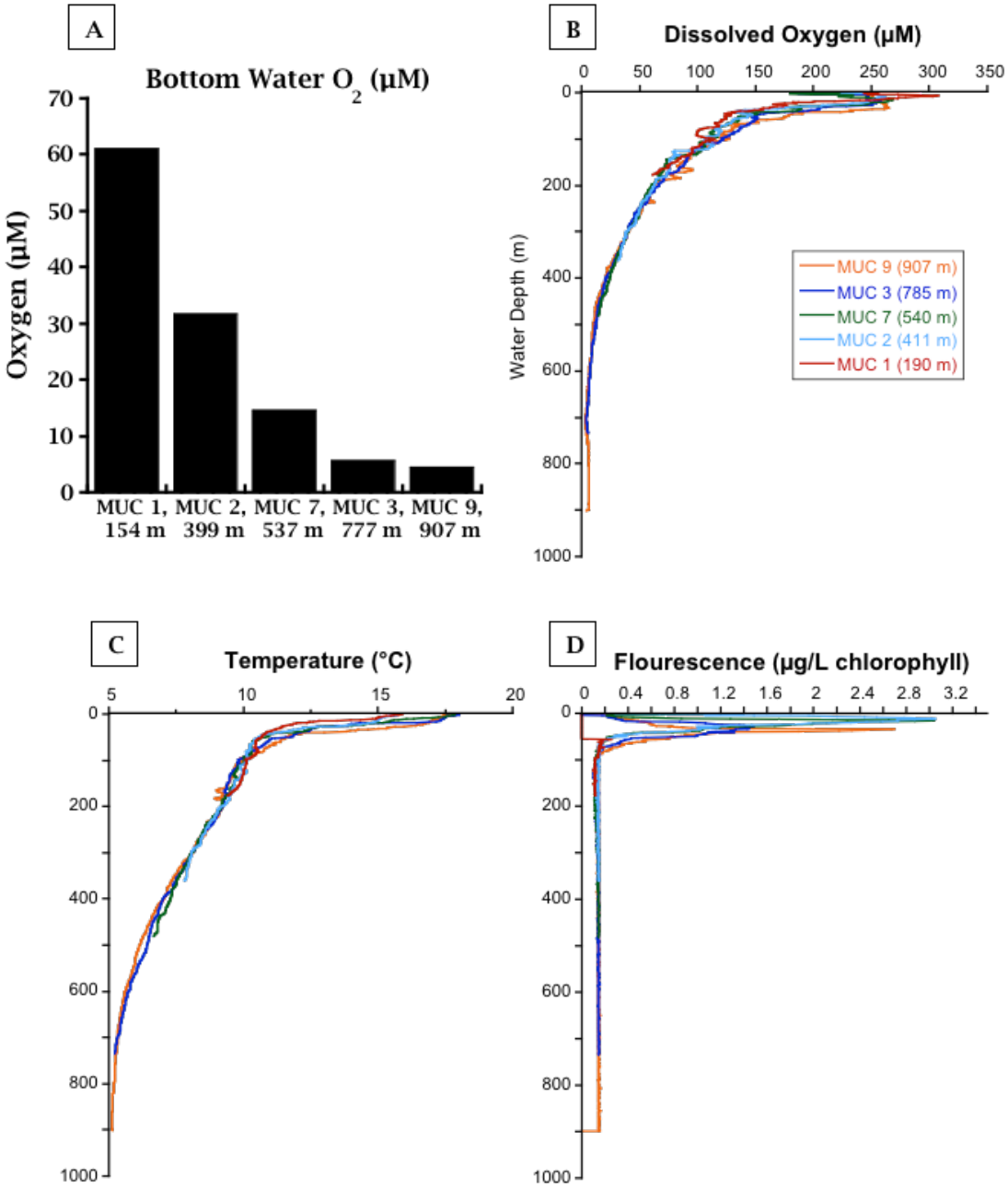

Figure 3-2: CTD casts. Bottom water dissolved oxygen (A, µM) and water column depth profiles of dissolved oxygen (B, µM), temperature (C, ˚C) and fluorescence (D, mg/L chlorophyll) for MUCs 1, 2, 7, 3 and 9. For water depths of bottom water oxygen values in (A) see Table 2-1.

3.3 Sediment porewater data

Geochemical profiles of sediment porewater ammonium (NH_4^+), ferrous iron (Fe (II)), phosphate (PO_4^{3-}), total sulfide (sulfide), sulfate (SO_4^{2-}), and total alkalinity (TA) are

shown in Fig. 3-3 for Transect 1 (MUCs 1-9) and Transect 2 (MUCs 10-12) from shallowest to deepest station. Individual values of all parameters are presented in the Appendix (Table 5-1). NO_3^- data, due to instrumental interferences, are excluded from this chapter and are discussed and shown in the Appendix (Table 5-2).

Fe (II) was undetectable in all station's supernatant water. The lowest porewater concentration was 1.1 µM at 154 m. Porewater concentrations of Fe (II) were highest in the two deepest stations, 132 and 175 µM, at 907 and 893 m, respectively. Shallow stations to intermediate depth stations (71 m to 537 m) showed a peak in Fe (II) towards the top of the core (< 5cm) and declined concentrations down core. Stations from 695 to 907 m showed intermediate to high concentrations mid core, until around 20 cm, where Fe (II) decreased, but never went to zero. The second deepest station, at 893 m, started to decline in Fe (II) concentrations shallower, at 13 cm. Additionally, at the 745 and 777 m stations, Fe (II) did not have a maximum peak in concentration within the top 5 cm of the core. At 695 m, Fe (II) concentrations were between 126 and 140 µM from 1.5 to 17 cm. At 745 m, concentrations were between 71 and 87 µM Fe (II) from 5 to 19 cm. Fe (II) peaked at 6, 9 and 11 cm, at 777 m, displaying a zigzag profile. At 907 m, Fe (II) was between 116 and 132 µM from 1.5 to 19 cm.

Core supernatant water concentrations of PO_4^{3-} for depths 154, 319 and 777 m (MUCs 1-3, respectively) were not measured. Supernatant concentrations in all other MUC cores ranged from 2.1 to 5.4 µM. The highest supernatant concentrations of 4.6 and 5.4 µM PO_4^{3-} were found at the two deepest stations, 893 and 907 m, respectively. These stations also exhibited the highest concentrations of and largest accumulation of PO_4^{3-} in the porewater down core. At 907 m, PO_4^{3-} concentrations decreased from 81 µM to 71.7 µM from 0.5 to 1.5 cm. PO_4^{3-} increased from 71.7 µM at 1.5 cm to 146 µM at 30 cm. At 893 m, PO_4^{3-} increased from 66.2 µM at 0.5 cm to 130.1 µM at 26 cm.

Concentrations of Fe (II) and PO_4^{3-} are important to consider together, because when Fe (III) is reduced to Fe (II), it releases PO_4^{3-}. Therefore, similar trends are expected for both Fe (II) and PO_4^{3-} until Fe (II) reacts with sulfide produced from sulfate reduction. Stations at 319, 399, 485 and 777 m showed PO_4^{3-} trends very similar to Fe (II) trends. At these stations maximum concentrations peaked at the top of the core and concentrations decreased down core. The second shallowest station at 154 m showed a large variability in the profile for PO_4^{3-} concentrations, with the lowest concentration of 11.6 at 0.5 cm and the highest concentrations of 138 at 9.5 cm and 117 at 7.5 cm. PO_4^{3-} at 695 and 745 m decreased while Fe (II) did not, whereas at every other station, Fe (II) decreased before PO_4^{3-} or concurrently with PO_4^{3-} concentrations. At 695 m, porewater PO_4^{3-} decreased from 4 to 10 cm, while Fe (II) remained constant at high concentrations for depths between 2 and 17 cm. At 745 m Fe (II) remained high for depths between 5 and 19 cm and PO_4^{3-} decreased from 9 to 22 cm.

NH_4^+ data for stations at 154, 399, and 777 m water depth (MUCs 1, 2, and 3) are possibly compromised due to sampling errors. We believe that the instrument was blanked with the highest standard, and therefore the standard curve from the subsequent run of NH_4^+ samples (stations at 319, 485 and 537 m) was used for stations at 154, 399 and 777m. However, while absolute values are likely not correct for the first three MUCs, we believe that general trends in profiles are trustworthy. The core supernatant water for all other stations contained undetectable levels of NH_4^+. NH_4^+ accumulated down core at station depths of 695, 745, 893 and 907 m with the highest concentration at the deepest station (328 µM at 26 cm). The two deepest stations showed the most linearity in the geochemical profiles of NH_4^+. At the 777 m station (MUC 3), NH_4^+ concentrations remained constant at ~30 µM until 19 cm, where NH_4^+ increased linearly until peaking at 134 µM at 30 cm. Similar to NH_4^+ profiles, TA

remained relatively constant (~ 2.5-3.5 mM) in all MUCs except at the deepest stations, 893 and 907 m, where TA increased to 5.5 mM at 30 cm and 7.3 mM at 30 cm, respectively. Stations at 777, 695 and 745 m showed constant profiles until ~15 cm where TA increased. All supernatants at all stations showed a TA concentration just below or at 2.5 mM.

SO_4^{2-} concentrations at all but the two deepest stations remained constant from the core supernatant water to the bottom of the core. SO_4^{2-} porewater concentrations varied from 24.3 to 28.9 µM at the 154 m station, displaying a zigzag profile. Porewater SO_4^{2-} concentrations at the deepest station (907 m) decreased from 27.8 µM at 1 cm to 24.8 µM at 30 cm. At 893 m, SO_4^{2-} decreased from 27.9 µM at 1 cm to 25.9 µM at 30 cm.

Total sulfide was undetectable in the supernatant of all cores, except at 907 m, sulfide was 45 µM. Porewater sulfide concentrations were overall low and constant throughout the cores, (0-5.2 µM). The only peaks in sulfide were found at 154 and 777 m where sulfide maximums occurred at 6.5 cm (11. 7 µM) and at 9.5 cm (54.7 µM). At the two deepest stations, sulfide did not reach zero in the sediment, but rather remained constant around 3 µM.

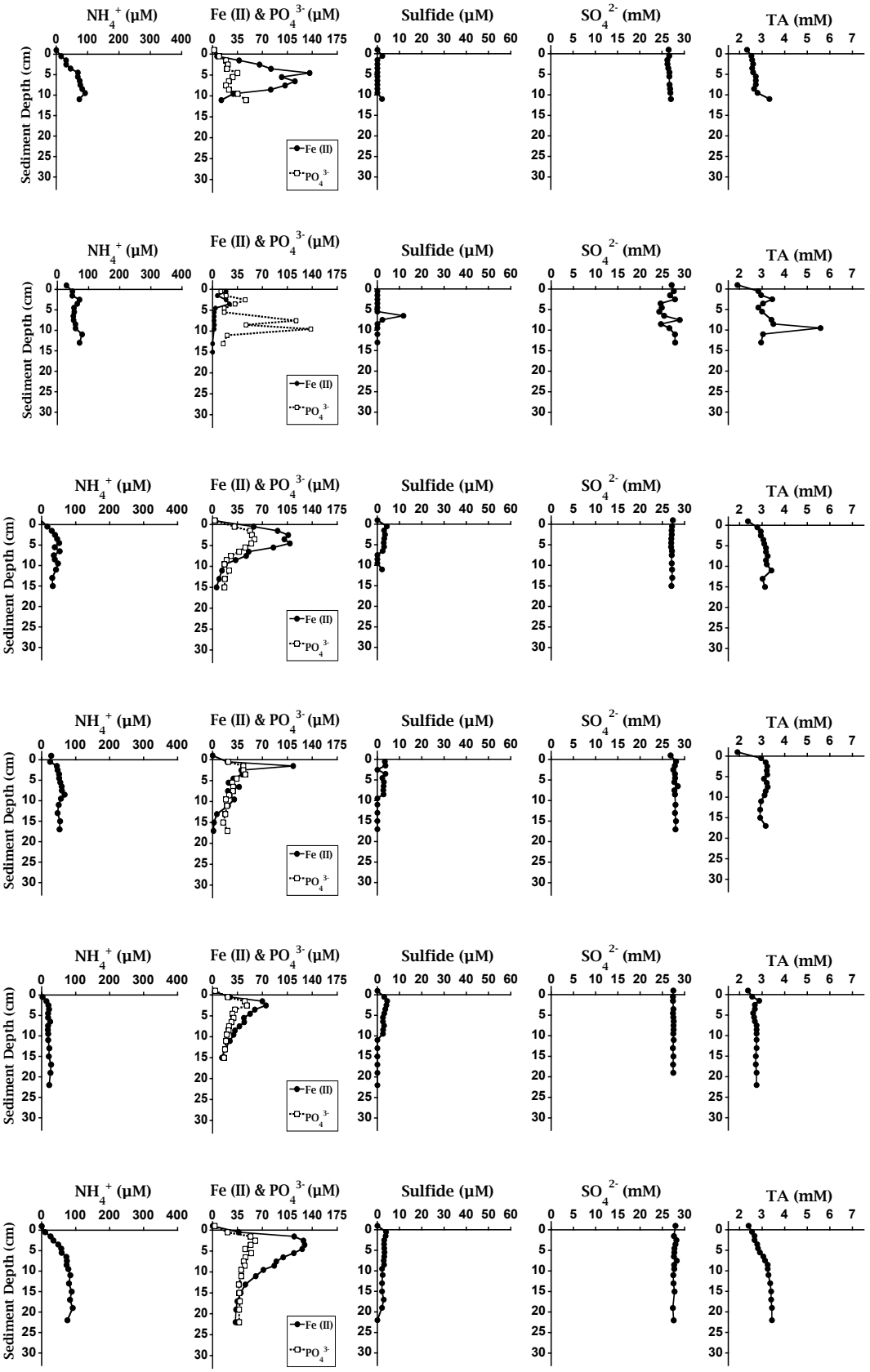
Transect 1
MUC 4, 71 m
MUC 1, 154 m
MUC 5, 319 m
MUC 2, 399 m
MUC 6, 485 m
MUC 7, 537 m
NH4+ (µM)
Fe (II) & PO43- (µM)
Sulfide (µM)
SO42- (mM)
TA (mM)
Sediment Depth (cm)
Fe (II)
PO43-

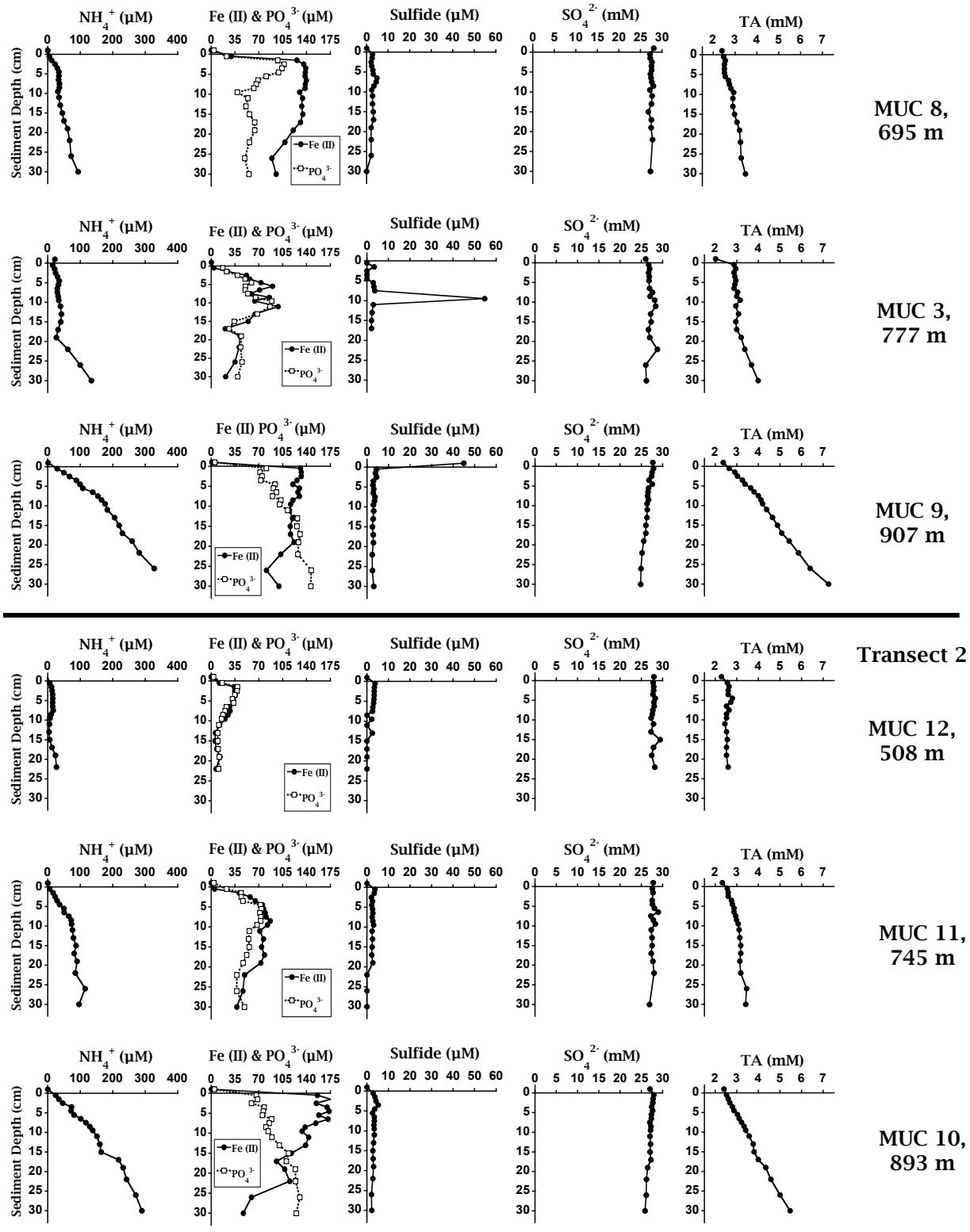

Figure 3-3. **Biogeochemical porewater profiles.** Porewater concentrations of ammonium (NH_4^+, µM), ferrous iron (Fe (II), µM), phosphate (PO_4^{3-}, µM), sulfide (µM), sulfate (SO_4^{2-}, mM), and total alkalinity (TA, mM) in sediments cores from Transect 1 and 2 organized from shallowest to deepest water depth.

3.4 Sulfate reduction

Sulfate reduction rates were overall low (0-5 nmol SO_4^{2-} cm^{-3} d^{-1}), with the exception of 62.3 nmol SO_4^{2-} cm^{-3} d^{-1} at 154 m station (3 cm; core replicate 2, Appendix, Table 5-3). The second highest rates were 17.3 nmol SO_4^{2-} cm^{-3} d^{-1} at 399 m (0.5 cm sediment depth) and 15.7 nmol SO_4^{2-} cm^{-3} d^{-1} at 907 m (0.5 cm sediment depth). The shallower to intermediate depth stations (71, 319, 399, 537, 695 and 745 m) all showed the most sulfate reduction activity mid-core. These stations also exhibited higher variability than the deeper stations, with the most variability at 399 m in both replicates. The station at 508 m showed hardly any sulfate reduction, with rates between 0.1 and 2.6 nmol SO_4^{2-} cm^{-3} d^{-1}. Only the three deepest stations at 777, 895 and 907 m, showed major sulfate reduction close to the sediment water interface (Fig. 3-4). The deepest station showed an exponential decline of sulfate reduction from 0.5 cm sediment depth to the bottom of the core. The second deepest station also showed an exponential decrease from the top of the core to 5.5 cm sediment depth. From 6.5 cm to 8.5 cm, sulfate reduction increased slightly, decreased at 9.5 cm and then increased again until 11.5 cm. Rates remained low, 0.8-3.3 nmol SO_4^{2-} cm^{-3} d^{-1}, from 12.5 cm to 24.5 cm. Replicate 2 at the 777 m station also showed an exponential decline from the top to the bottom of the core. Replicate 1 showed a bit more variation, with peaks at 1.5 cm and 7.5 cm. Additionally, stations at 695 and 745 m showed concave profiles, with maxima rates of 6 and 4.8 nmol SO_4^{2-} cm^{-3} d^{-1} at 11.5 and 13.5 cm, for 695 and 745 m, respectively.

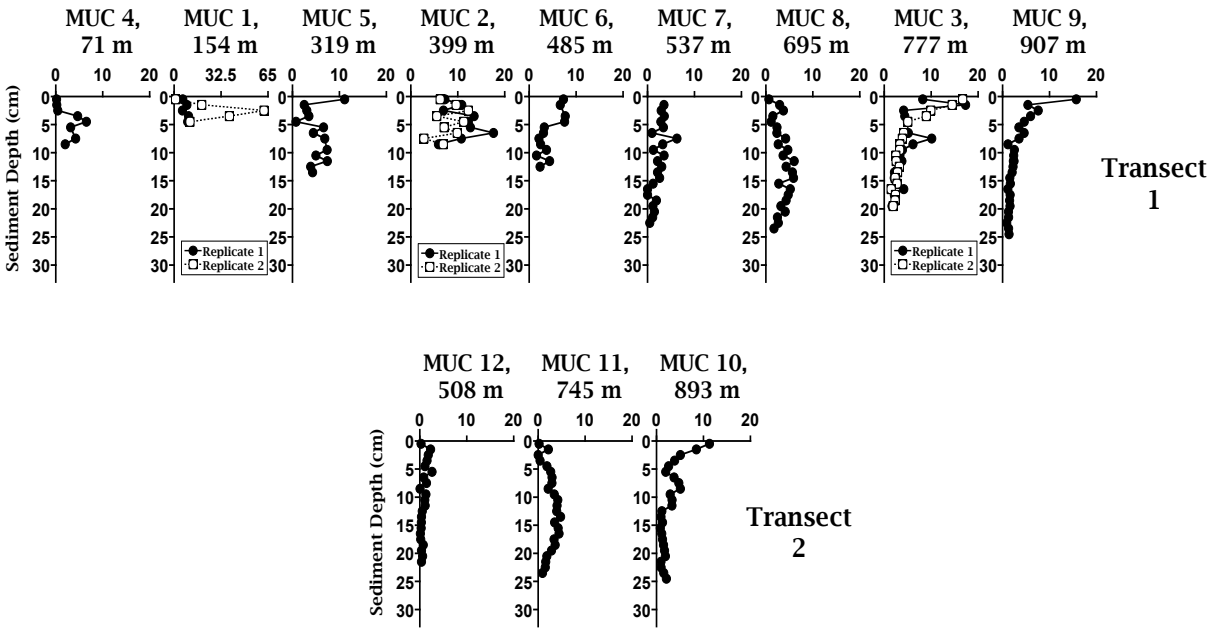

Figure 3-4: Sulfate reduction. Depth profiles of sulfate reduction rates (nmol SO_4^{2-} cm^{-3} d^{-1}) for all stations. Top: Transect 1 (MUCS 1-9) from shallowest to deepest station. Bottom: Transect 2 (MUCs 10-12) from shallow to deep. X-axis for MUC 1 extends to 65 µM to show highest sulfate reduction in replicate 2.

Sulfate reduction rates for each station were integrated over a 10 cm core depth, except for stations at 71 m and 154 m, which were integrate over 9 cm and 5 cm, respectively (Fig. 3-5). Additionally, MUCs 1-3 each had a replicate core. The highest integrated sulfate reduction was seen at the 154, 399 m stations (MUC 1 and MUC 2; 0.86 and 0.85 mmol m^{-2} d^{-1}, respectively). The next highest integrated rates of 0.67, 0.5 and 0.55 mmol m^{-2} d^{-1} were seen at the three deepest stations: 777, 893 and 907 m, respectively. The intermediate depth station at 508 m station had the lowest rate of 0.13 mmol m^{-2} d^{-1}.

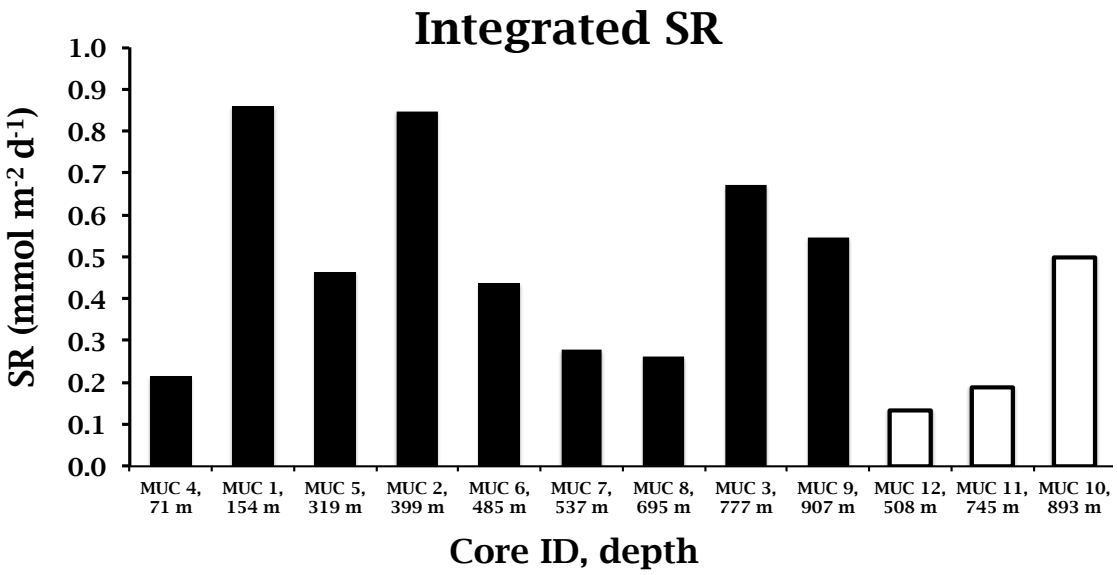

Figure 3-5: **Integrated sulfate reduction rates.** Integrated sulfate reduction rates (mmol m^{-2} d^{-1}) for Transect 1 (black) and 2 (white). All cores were integrated over a 10 cm depth, except for stations at 154 m (5-cm integration depth) and 71 m (9-cm integration depth) due to short cores.

4 Discussion

This study provides geochemical and biological information on the benthic environment of the Santa Monica Basin, California. We hypothesized that the Santa Monica Basin (SMB) oxygen minimum zone (OMZ) has expanded since Gorsline (1992) reported the trend of increasing near anoxia over the previous 350 years. Such an increase near anoxia would be important as it might lead to (1) iron and phosphorous releases from the seafloor into the water column, (2) increased bacterial sulfate reduction in the sediment as compared to other, less productive environments, and (3) an absence of bioturbation in sediment cores retrieved from shallower than 830 m water depths. In the following, the hypotheses will be compared with the data and discussed.

4.1 Distribution of O_2 in the Santa Monica Basin

Surface O_2 concentrations were high at all five CTD stations along Transect 1 (~272 µM O_2), due to photosynthesis producing O_2 in the upper water column and atmospheric exchange with the surface ocean. The peak in fluorescence between 10 and 50 m below sea level indicated the highest abundance of photosynthetic organisms at that depth. Dissolved O_2 data showed declining bottom water concentrations with increasing water depth of the stations (Fig 3-2). The start of the decline occurred just after the sharp decline in fluorescence, representing the beginning of the respiration zone (Fig. 3-2). Unlike the open ocean, the SMB is a closed basin system at depth, limiting O_2 replenishment from surrounding basins (Berelson, 1991). Therefore, after O_2 is consumed by respiration of organic matter, hypoxic conditions reach to the deepest parts of the basin. The higher bottom water O_2 concentrations seen at the shallower stations are probably a result of more wind-induced vertical mixing of

surface oxygenated waters with depleted O_2 water at depth. The dissolved O_2 never reached complete anoxia (0 µM O_2), even at the deepest station of 907 m (4.4 µM O_2). The near-anoxic condition of the deep basin could be a result of temporal flushing of the basin, which has been documented to occur every few years in neighboring basins (Berelson, 1991). An 11-year time series of temperature, salinity and nutrients for the San Pedro and San Nicolas Basins, adjacent to the Santa Monica Basin revealed a flushing event in the basins between 1982-1984 followed by a period of stagnation between 1984-1987. During the flushing period, the O_2 in the San Pedro Basin increased from 3-5 µM to ~15 µM O_2, and temperature decreased 0.2˚C (Berelson, 1991).

4.2 Bioturbation

Laminations are small-scale sequences of fine layers of deposited sediment (Blatt et al., 2006). According to Kemp (1996) laminations develop under two fundamental requirements: (1) compositional changes in the sediment due to variation in chemical/biological activity; and (2) preservation of the laminated sediment fabric due to the absence of bioturbation. In highly productive marine systems, reduced O_2 in anoxic silled basins (e.g. California Borderland basins) or marginal seas (e.g. Black Sea) is the dominant control on lamina preservation (Kemp, 1996). Low O_2 environments (<10 µM O_2) exclude benthic macrofauna, and therefore bioturbation is limited under O_2-depleted conditions. Bioturbation, an animal-induced disruption of lamina, can displace organic matter, electron acceptors and microorganisms both laterally and vertically, creating zigzag geochemical profiles (Kristensen et al., 2012). Because the deepest parts of the SMB are free of bioturbation (Christensen et al., 1994; Gorsline et al., 1992), sediments from the basin have been the focus for many investigations (e.g., Jahnke, 1990; Christensen et al., 1994; Gorsline, 1996, 1992; Gong and Hollander,

1999; Masiello and Druffel, 2003; Prokopenko et al., 2011; Komada et al., 2013; Monteverde et al., 2015). The laminated sediment have been used as a high-resolution archive of paleoceanographic proxies (Christensen et al., 1994; Gorsline, 1992, 1996), to measure the recycling and burial rates of organic carbon at the seafloor (Jahnke, 1990; Komada et al., 2013, 2016) and to assess the role of bottom water O_2 in preserving organic matter and the differential contribution of bacteria to the sedimentary organic matter (Gong and Hollander, 1999). Similar to the Santa Monica Basin, the Santa Barbara Basin also exhibits sediment laminations in the deepest parts of the basin, below ~525 m (Behl et al., 1996). In this neighboring basin, sub annual oxygenation events were not enough to allow bioturbation. I propose that the oxygen levels at our two deepest stations (~ 5µM, 893 and 907 m) were not enough for macrofauna to exist. The O_2 threshold for bioturbation has been studied extensively. Calvert (1964) found laminations at 8.93 µM O_2, Savrda et al (1984) found laminations at 6.7 µM O_2, and Thompson et al., (1985) suggestd that the preservation of laminations occurs only below 4.46 µM. A study performed by Gong and Hollander (1997) showed that in the SMB depocenter (~900 m) laminations were found at bottom water O_2 levels at or below 4.5 µM O_2. Our findings for the SMB suggest that bioturbation is absent at bottom water O_2 levels <5.6 µM, but is present at bottom water O_2 of 15 µM O_2 (Fig. 3-2; Fig. 3-3). However, because we do not have data from sediment cores with O_2 levels between 5.6 and 15 µM, more sediment cores should be analyzed between the 893 m and 777 m stations for more specific thresholds of O_2 for bioturbation in the SMB.

Our results showed that at the two deepest stations (893 and 907 m), NH_4^+ and TA increased linearly down core, as compared to non-trending or zigzag profiles at all other stations (Fig. 3-3). In anoxic sediment, organic carbon degradation processes such as denitrification and sulfate reduction produce bicarbonate (HCO_3^-), which

increases TA. Microbial organic matter degradation also releases NH_4^+ when particulate organic N is degraded (via ammonification). The accumulation of TA and NH_4^+ in the deepest stations therefore indicates anaerobic degradation processes. The linear geochemical profiles also indicate non-bioturbated sediments. Compared to the other cores, the 893 and 907 m stations showed high ex-situ rates of sulfate reduction and high concentrations of Fe (II), an indication for iron reduction, confirming the accumulation of TA and NH_4^+ and near-anoxia conditions at the sediment-water interface at these depths. Additionally, a decreasing exponential ^{210}Pb profile (W. Berelson, unpubl. data) at the deepest station affirms the absence of bioturbation. In contrast, all of the shallower cores showed clear signs of bioturbation. Importantly, at the third deepest station (777 m), NH_4^+ concentrations remained unchanged until 19 cm, pointing to sediment mixing processes. Similarly, Stations at 777, 695 and 745 m showed unchanged TA concentrations until ~15 cm. Evidence of bioturbation was therefore seen starting somewhere between 893 and 777 m water depth.

4.3 Iron and phosphorous fluxes into the water column

In the presence of O_2, dissolved Fe (II) is oxidized to solid iron mineral forms, which have a very high affinity for adsorption of anions like PO_4^{3-}. If iron oxidation occurs, the PO_4^{3-} becomes trapped from escaping into the shallower water depths (Jørgensen, 2006). Anoxic bottom water conditions permit reduced iron (and thus PO_4^{3-}) to escape into the above water column, providing important feedbacks to the surface-water primary productivity (Wallman, 2003). As an example, the Peruvian OMZ (<2 µM O_2) average PO_4^{3-} flux exceeds the average global flux from oxic shelf and slope environments by a factor of 17 (Noffke et al., 2012). Average benthic in situ PO_4^{3-} fluxes of 97 µmol m^{-2} d^{-1} at ~5 µM O_2 were measured in the SMB (Jahnke, 1990). Additionally, a

chamber study in the Santa Monica and San Pedro Basins showed a high Fe (II) flux at 900 m (4 µM O_2) of ~415 µmol m^{-2} d^{-1} (Severmann et al., 2010). This flux was higher than the one predicted by porewater Fe (II) gradients by Elrod et al. (2004) (275 µmol m^{-2} d^{-1}). The flux measured by Elrod et al. (2004) was correlated with higher O_2 concentrations near the seafloor (9-10 µM O_2).

We would expect fluxes of both Fe (II) and PO_4^{3-} into the core supernatant water of our cores because we also reported low O_2 concentrations of ~5 µM for our deepest stations. Core supernatant water concentrations of PO_4^{3-} for depths 154, 319 and 777 m were not measured, but supernatant concentrations of PO_4^{3-} at all other stations ranged from 2.1 to 5.4 µM. The highest supernatant concentrations of 4.6 and 5.4 µM PO_4^{3-} were found at the two deepest stations: 893 and 907 m, respectively. Our results showed that while we did measure PO_4^{3-} concentrations in the supernatant waters, concentrations of Fe (II) were below detection at all stations. Undetectable Fe (II) concentrations indicate four possibilities: (1) there were fluxes of Fe (II) into the water column but our data did not show the fluxes because of dilution in the water column, (2) there were Fe (II) fluxes but our data did not show them because O_2 introduction when sampling caused an oxidation in the water column and (3) there were no fluxes of Fe (II) into the water column because the natural O_2 in the water was sufficient to oxidize Fe (II). (4) If the 4.4 µM O_2 concentration was enough to oxidize the Fe (II), the sulfide produced in sulfate reduction locked up the Fe (II), leaving PO_4^{3-} to escape into the water column (Canfield, 1989). Given the studies cited above (Jahnke, 1990; Elrod et al., 2004), oxidation is unlikely since we reported 4.4 µM O_2. Based on our oxygen optode readings (Fig. 2-4) we think that O_2 was possibly introduced into the cores when the cores were capped with rubber stoppers on the boat. If so, the newly introduced oxygen could have artificially oxidized Fe (II), especially because Fe (II) is very sensitive

to O_2. Because of this possible artificial oxidation influence, we cannot fully refute our first hypothesis that iron and phosphorous releases from the seafloor into the water column would occur in stations shallower than 830 m.

4.4 An unusual iron story

According to the redox cascade, iron-reduction precedes sulfate reduction because of its higher energy gain (Jørgensen, 2006). However, it has been suggested that the typical order of electron acceptors (oxygen, nitrate, manganese, iron, sulfate and carbon dioxide) isn't absolute and reduction can occur in close association with each other or even in inverse sequence (Riedinger et al., 2017; Treude et al., 2014). Although we did not directly measure iron reduction, the iron reduction zone can be inferred where a peak in Fe (II) occurs, typically followed by a decline in Fe (II) down core, marking the transition to the sulfate reduction zone. In all cores, the inferred iron reduction zone was fairly shallow (<5 cm), except for the stations at 745 and 777 m. At 777 m, Fe (II) peaks at 6, 9 and 11 cm. At 745 m, high concentrations of Fe (II) were observed from 5 to 19 cm. The multiple peaks and constant high concentrations could be due to bioturbation (1) displacing iron reducing microorganisms deeper into the sediment and/or (2) pushing enhanced organic matter availability deeper (Kristensen et al., 2012). Adhering to the typical redox cascade, an iron reduction zone, defined by a peak in Fe (II), was seen shallower than the sulfate reduction zone for intermediate depth stations at 399, 508, 537, 695, and 745 m. In contrast, a peak in Fe (II) was seen deeper than the sulfate reduction zone for stations at 154, 319, 485, 777 and 893 m, suggesting that iron reduction occurred after sulfate reduction at these stations. Fe (II) high concentrations and sulfate reduction overlapped at the shallowest (71 m) and deepest (907 m) stations. Experimental data from various sedimentary

environments indicate that reduction of Fe (III) and sulfate can happen concurrently, or can even be reversed, based on the stability of iron oxides and the pH of the sediment (Postma and Jakobsen, 1996). The deepest station at 907 m showed a clear peak in Fe (II) concentration and the highest rate of sulfate reduction at 1 cm. However, the sulfate reduction immediately decreased, whereas Fe (II) remained constant until 19 cm. The constant high concentration of Fe (II) at 907 m shows that Fe (II) did not react with sulfide from 1–19 cm. Instead, high Fe (II) throughout the deepest cores at 893 and 907 m indicates an expansion of the iron reduction zone.

The station at 695 m showed a sink for porewater PO_4^{3-} from 4 to 10 cm, while Fe (II) remained constant at high concentrations for depths between 2 and 17 cm. This also occurred at 745 m where Fe (II) remained high for depths between 5 and 19 cm and PO_4^{3-} decreased from 9 to 22 cm. At these stations, the PO_4^{3-} could have re-adsorbed onto particle surfaces, co-precipitated with in-site formed minerals, or formed authigenic carbonate fluorapatite (Jørgensen, 2006).

4.5 Interpretation of sulfate reduction and iron-sulfide compounds

According to Jørgensen (1978), classical sulfate reduction rates in marine shelf systems are on the order of 1-100 nmol cm^{-3} d^{-1}. Typical integrated sulfate reduction rates in surface sediments (0-30 cm) within OMZs range between 1 and 60 mmol m^{-2} d^{-1} (Fossing 1990; Brüchert et al. 2003; Ferdelman et al. 1997; Fossing et al. 2000). Sulfate reduction rates of ~10 nmol cm^{-3} d^{-1} were reported along the Chilean continental margin (Treude et al., 2005) and integrated sulfate reduction rates reported in the Black Sea range from 0.04 to 5.6 mmol m^{-2} d^{-1} (Sorokin, 1962; Vaynshteyn et al., 1985; Lein et al., 1991). Because SO_4^{2-} is so abundant in the marine system, sulfate reduction usually dominates over all other anaerobic degradation processes in the

sediments, especially in shallower, more productive depositional settings (Jørgensen, 2006). Our results showed a maximum sulfate reduction rate of 62.3 nmol SO_4^{2-} cm^{-3} d^{-1} at 154 m at 3 cm in the core. The second highest rates were 17.3 nmol SO_4^{2-} cm^{-3} d^{-1} at 399 m at 0.5 cm in the core and 15.7 nmol SO_4^{2-} cm^{-3} d^{-1} at 907 m at 0.5 cm in the core. Although these three maxima fall within normal sulfate reduction rates according to others, the majority of the rates were at or below 5 nmol SO_4^{2-} cm^{-3} d^{-1} (Appendix, Table 5-3). Integrated rates were between only 0.13 – 0.86 mmol m^{-2} d^{-1}. The three deepest stations at 777, 907 and 893 m showed major peaks in sulfate reduction close to the sediment water interface, indicating anoxic sediment. Highest sulfate reduction integrated over the top 10 cm of sediment occurred at depths of 154, 319 and 777 m (Fig. 3-5). For the two shallower stations of 154 and 319 m, we would expect to see lower integrated rates of sulfate reduction over the sampled depths since more O_2 enters the sediment at these stations due to higher concentrations of O_2 in the water column, more permeable (less porous) sediment, and more wave action (Huettel et al., 2014). The high-integrated rates at these stations compared to the other stations could be a result of bioturbation vertically displacing the solutes, organic matter and/or sulfate-reducing microorganisms, causing the integrated sulfate reduction to appear higher. However, the integrated rates at all stations were still low compared to other reports (Fossing 1990; Brüchert et al. 2003; Ferdelman et al. 1997; Fossing et al. 2000). Additionally, the low ex-situ sulfate reduction rates do not support hypothesis number two, that we would find high sulfate reduction rates underlying a near-anoxia water column. The majority of sulfate reduction at the deepest stations was however, close to the sediment-water interface, reflecting typical sulfate reduction zones underlying low O_2 waters. Overall low sulfate reduction rates in the SMB could be a result of different processes.

Typically, with increasing depth in the sediment, SO_4^{2-} decreases due to sulfate reduction, and sulfide is produced, often creating distinct peaks in the sulfide profile. Sulfide can then either react with Fe (II) to form iron-sulfide compounds, such as iron mono sulfide (FeS), or if sulfur bacteria are present, it can be re-oxidized to SO_4^{2-} (Jørgensen, 2006). We would expect to see high rates of sulfate reduction in our sediment cores compared to other, less productive environments with plenty of O_2 in the water column, but not necessarily higher rates in our deeper stations compared to our shallower stations. The amount of organic carbon that reaches the seafloor decreases with increasing water depth, therefore at shallower depths, there is more organic matter available for degradation processes such as sulfate reduction. We would also expect to see Fe (II) reacting with sulfide produced in sulfate reduction forming iron-sulfide compounds. Overall sulfide concentrations were low (0-5.3 µM sulfide), except for an unusually high supernatant concentration of sulfide at the deepest station of 45 µM. Because sulfide only diffuses into the water in complete anoxia, we do not trust this value, as we had 4.4 µM O_2 in the bottom water. The sulfide was possibly stirred up through the sediment when we pushed the core down onto the core stopper or the extruder. At the two deepest stations, where iron-sulfide compound formation was expected, sulfide did not reach zero, nor did it develop distinct peaks in the cores. Furthermore, Fe (II) did not substantially decline, but remained relatively high where sulfide was low, but present (Fig. 3-3). Our results of non-zero sulfide at the deepest stations were substantiated by reported low pyrite formation at 907 m (~0.13 FeS_2 wt.%) and 893 m (~0.091 FeS_2 wt.%) (T. Lyons, unpubl. data). Additionally, high reactive iron phases (i.e. Fe (III)) and high total organic carbon (TOC) content at 907 m (5 %) and 893 m (5.2 %) (T. Lyons, unpubl. data) were reported at these two stations. Typically, high TOC in a near-anoxic region would suggest high sulfate reduction

activity, since sulfate reduction is the dominant anaerobic degradation process. The observed low sulfate reduction rates, however, could suggest that the organic matter was refractory. C/N ratios, a proxy for the freshness of organic matter, would help us understand if the organic matter is past its labile phases, remaining unattractive to microorganisms.

Profiles of TA, SO_4^{2-}, PO_4^{3-}, NH_4^+ and Fe (II) in the central SMB (~5 µM O_2) measured 30 years ago, were very similar to our results (Fig. 3-3) (Jahnke, 1990). Jahnke (1990) concluded that the low ratio of porewater TA production to the net consumption of sulfate couldn't be explained by organoclastic sulfate reduction following Redfieldian ratio. He also showed that 12% of the TA flux originated from mineralization of the less reactive organic matter occurring at sediment depths greater than 40 cm. More recently, Burdige and Komada (2011) found low ratios of porewater dissolved inorganic carbon (DIC) to sulfate consumption from organoclastic sulfate reduction at the same site, similar to Jahnke (1990), and proposed that the low ratio was linked to anaerobic oxidation of methane (AOM) in the deeper sediment (>1.2 m).

$$CH_4 + SO_4^{2-} \rightarrow HCO_3^- + HS^- + H_20 \quad (1)$$

I compared the sulfate flux from the integrated sulfate reduction to the theoretical sulfate flux, assuming a linear sulfate depletion over depth, using Fick's First Law (Krom and Berner, 1980):

$$J = D_0 \phi^3 (\partial C / \partial x) \quad (2)$$

for the two deepest stations at 907 and 893 m (24-cm sediment depth). Where D_0 is the diffusion coefficient of SO_4^{2-} in seawater (0.5 x10^{-5} cm^2 s^{-1} at 5˚C; Iversen and Jørgensen, 1993) and ϕ is the average porosity (0.867, 907 m and 0.816, 893 m). $\partial C/\partial x$ is the change in concentration of SO_4^{2-} over the change in sediment depth. For 907 m, the change in SO_4^{2-} concentration was 2.95 mM over 24.5 cm sediment depth. For 893 m,

the change in sulfate concentration was 1.79 mM over 24.5 cm sediment depth. The rate-based sulfate flux for the deepest station was 0.029 mmol cm^{-2} d^{-1} and the theoretical sulfate flux using Fick's Law was 0.013 mmol cm^{-2} d^{-1}; 2.2 times less than the rate-based flux. For the second deepest station, the rate-based sulfate flux was 0.027 mmol cm^{-2} d^{-1} and the theoretical sulfate flux was .006 mmol cm^{-2} d^{-1}; 4.5 times less than the rate-based flux of sulfate. The actual sulfate reduction is masked in the diffusive profile because most of the sulfate reduction activity is located close to the sediment-water interface, where sulfate is replenished quickly (Jørgensen et al., 2001)., It appears that the observed sulfate profile is governed by anaerobic oxidation of methane at depth (Niewöhner, 1998). AOM has been observed in the deep SMB sediments below 1.2 m (Komada et al., 2016).

Our low sulfate reduction rates and low iron-sulfide compound formation could also be a result of sulfur-oxidizing bacteria (e.g., *Beggiato*a and *Thioploca*) masking the true rates of sulfate reduction by oxidizing the sulfide produced in sulfate reduction (Canfield et al., 2010; Preisler et al., 2007). *Beggiatoa* mats were widely observed in the neighboring Santa Barbara Basin, and the chemoautrophic bacteria have been attributed to the increased TOC content in the region (Grant, 1991). In the SMB specifically, Christensen et al., (1994) and Reimers et al., (1990) suggested that *Beggiatoa* mat growth is the cause for sediment laminations. Gong and Hollander (1997) quantitatively assessed the role of bacteria and bottom water oxygenation in controlling the quality and quantity of organic matter in the sediments of the SMB. They concluded that anoxia provides a condition for slower decomposition of organic matter, and promotes the development of chemoautrophic bacteria, which could modify the chemical characteristics of the organic matter and increase the TOC accumulation (Gong and Hollander, 1997). These bacteria could explain our high TOC

content, though large, filamentous sulfide-oxidizing bacteria were not seen in or on any of our sediment cores. Although *beggiatoa* have been noted in the SMB sediments before (Grant, 1991; Christensen et al., 1994 and Reimers et al., 1990) it is difficult to assess if chemoautotrophic bacteria were in our sediment cores, based on these results. Our rate-based fluxes of sulfate were much larger than the theoretical sulfate fluxes at both station depths. If sulfide oxidation were occurring, we would expect to see a smaller rate-based sulfate flux, due to the re-oxidation of the sulfate tracer during incubation.

4.7 Overall conclusions and outlook

According to the stations sampled, we could not identify a definite spreading or reduction of the SMB OMZ at the seafloor since the last survey of the region ~35 years ago. The undisturbed geochemical profiles and the absence of macrofauna at the two deepest stations at 893 and 907 m (Fig. 3-3) are a good indication of near-anoxic bottom water conditions, underlying high biological productivity in the surface ocean. The accumulation of degradation products (TA and NH_4^+) and the presence of high peaks in Fe (II) and sulfate reduction at these stations, suggest that there is clear organic matter deposition and anaerobic degradation. Laminations seen in X ray images and exponential ^{210}Pb profiles for these stations (W. Berelson, unpubl. data) verify the lack of bioturbation. Sulfate reduction activity was present, but low at all stations along the depth transects. All reduced dissolved species (Fe (II), NH_4^+, and sulfide) were absent in the core supernatant waters, with the exception of sulfide at the deepest station (see section 4.5), resulting from either enough O_2 present to oxidize the chemical solutes, artificial oxidation from transporting the sediment cores, or dilution. Fe (II) could have also bound with sulfide produced from sulfate reduction, although

our high concentrations of Fe (II) in the deepest cores don't support iron-sulfide compound formation, but rather a persisting iron reduction zone. Because others have reported Fe (II) fluxes into the water column in the SMB under the same or higher bottom water O_2 conditions than we reported (Jahnke, 1990; Elrod et al., 2004), it is more plausible that there were indeed Fe (II) fluxes into the water column, but artificial oxidation occurred.

Additional fieldwork and analyses are necessary for understanding the biogeochemical system in the Santa Monica Basin. First, a replication of our analyses, including deeper sediment (gravity) cores with additional stations is integral to understanding the full redox system. This would provide an insight into how the redox cascade continues deeper into the sediment. Because the absolute values of our PreSens O_2 sensor optodes were unreliable, a more accurate inventory of DO in the sediment cores is necessary to evaluate the O_2 threshold for macrofauna and reduced solutes in the SMB. In order to investigate the unreactive organic matter hypothesis, Fe (III), solid sulfur phases, sulfate reduction, sulfur isotopes, and C/N analyses should be further explored (Riedinger et al., 2017). Riedinger et al. (2017) suggested that abundant reactive iron phases and refractory organic matter may result in low sulfate reduction. They also showed that in non-steady state systems, redox zones do not necessarily occur in sequence, but can reappear or become inversed. Another interesting idea, of more recent attention, is iron-mediated anaerobic oxidation of methane (AOM) (Riedinger et al., 2017). Our cores were not deep enough to detect AOM, since in diffusive systems this zone usually exists one to several meters below the sea surface (Jørgensen, 2006).

5 Appendix

Table 5-1: Porewater analyses. Core ID, date, and location for MUCs 1-12 for iron (II) (µM), phosphate (µM), ammonium (µM), total alkalinity (mM) total sulfide (µM) and sulfate (mM).

Core ID	Date	Water depth (m)	Sediment depth (cm)	Iron (II) (µM)	Phosphate (µM)	Ammonium (µM)	TA (mM)	Sulfide (µM)	Sulfate (mM)
MUC 1	5/26/17	154	supernatant	0.0	-	-	2	-	27.1
MUC 1	5/26/17	154	0.5	3.8	11.6	48.3	2.8	0	27.6
MUC 1	5/26/17	154	1.5	3.4	19.1	47.5	2.9	0	26.7
MUC 1	5/26/17	154	2.5	3.8	45.9	71.1	3.4	0	27.8
MUC 1	5/26/17	154	3.5	4.7	31.6	63.5	3.0	0	24.6
MUC 1	5/26/17	154	4.5	2.0	16.3	53.2	2.8	0	24.9
MUC 1	5/26/17	154	5.5	1.3	16.3	54.0	3.0	0	24.3
MUC 1	5/26/17	154	6.5	1.2	-	50.9	-	11.7	25.4
MUC 1	5/26/17	154	7.5	1.1	117.2	52.1	3.4	2.3	28.9
MUC 1	5/26/17	154	8.5	1.3	46.8	57.8	3.5	0	24.7
MUC 1	5/26/17	154	9.5	1.1	137.9	58.2	5.6	0	26.6
MUC 1	5/26/17	154	11.0	-	20.5	79.2	3.0	0	27.8
MUC 1	5/26/17	154	13.0	-	14.9	71.1	2.9	0	27.9
MUC 2	5/26/17	399	supernatant	0.0	-	-	1.9	-	26.8
MUC 2	5/26/17	399	0.5	20.7	22.1	25.0	2.9	3.4	28.1
MUC 2	5/26/17	399	1.5	113.2	43.2	44.5	3.2	3.6	27.8
MUC 2	5/26/17	399	2.5	40.2	43.2	46.8	3.2	0	27.5
MUC 2	5/26/17	399	3.5	41.9	45.9	50.9	3.2	3.6	27.8
MUC 2	5/26/17	399	4.5	29.2	33.9	51.3	3.2	2.3	27.8
MUC 2	5/26/17	399	5.5	22.4	27.7	54.8	3.1	2.9	27.7
MUC 2	5/26/17	399	6.5	37.2	28.9	58.6	3.2	2.8	28.5
MUC 2	5/26/17	399	7.5	21.5	28.6	59.3	3.2	2.7	27.7
MUC 2	5/26/17	399	8.5	24.1	23.1	67.3	3.2	2.8	27.8
MUC 2	5/26/17	399	9.5	30.5	18.6	56.7	3.1	0	-
MUC 2	5/26/17	399	11.0	21.8	20.4	50.2	2.9	0	28.0
MUC 2	5/26/17	399	13.0	6.1	18.1	46.8	2.9	0	27.8
MUC 2	5/26/17	399	15.0	2.1	14.8	54.0	2.9	0	28.1
MUC 2	5/26/17	399	17.0	1.2	21.0	52.5	3.2	0	27.9
MUC 3	5/26/17	777	supernatant	0.4	-	-	2.0	-	26.0
MUC 3	5/26/17	777	0.5	3.7	17.0	14.7	2.9	0	26.7
MUC 3	5/26/17	777	1.5	24.3	22.6	21.2	2.9	3.4	26.9
MUC 3	5/26/17	777	2.5	51.7	38.5	23.9	2.9	0	26.7
MUC 3	5/26/17	777	3.5	56.5	49.9	30.0	2.9	0	26.8
MUC 3	5/26/17	777	4.5	73.0	59.2	35.3	2.9	0	26.8
MUC 3	5/26/17	777	5.5	90.1	50.3	32.6	2.9	2.9	-
MUC 3	5/26/17	777	6.5	71.2	49.9	29.2	2.9	3.2	26.9
MUC 3	5/26/17	777	7.5	58.0	53.9	29.6	3.0	3.6	27.6

MUC 3	5/26/17	777	8.5	85.4	65.1	31.9	3.0	-	27.1
MUC 3	5/26/17	777	9.5	63.9	89.0	33.8	3.2	54.7	28.1
MUC 3	5/26/17	777	11.0	98.4	86.3	39.1	2.9	2.9	28.4
MUC 3	5/26/17	777	13.0	64.4	67.8	42.2	3.1	2.4	27.2
MUC 3	5/26/17	777	15.0	54.5	33.9	39.9	2.9	2.1	27.3
MUC 3	5/26/17	777	17.0	20.5	26.4	31.5	3.0	2.1	26.7
MUC 3	5/26/17	777	19.0	42.3	44.2	26.5	3.2	0	27.0
MUC 3	5/26/17	777	22.0	41.2	43.2	61.6	3.4	2.1	28.8
MUC 3	5/26/17	777	26.0	35.0	45.3	99.7	3.7	0	26.0
MUC 3	5/26/17	777	30.0	21.3	38.9	134.0	4.0	2.5	26.5
MUC 4	7/13/17	71	supernatant	0.0	2.1	0.0	2.3	0	26.6
MUC 4	7/13/17	71	0.5	6.3	9.2	15.5	2.5	2.2	26.2
MUC 4	7/13/17	71	1.5	37.2	19.0	31.3	2.6	0	26.2
MUC 4	7/13/17	71	2.5	65.9	21.6	31.3	2.6	0	26.4
MUC 4	7/13/17	71	3.5	82.0	20.3	45.6	2.6	0	26.7
MUC 4	7/13/17	71	4.5	136.3	34.9	68.8	2.6	0	26.6
MUC 4	7/13/17	71	5.5	97.0	28.3	68.4	2.7	0	-
MUC 4	7/13/17	71	6.5	115.7	22.7	74.6	2.7	0	26.7
MUC 4	7/13/17	71	7.5	101.8	18.9	76.6	2.7	0	26.8
MUC 4	7/13/17	71	8.5	81.6	22.8	82.8	2.6	0	26.9
MUC 4	7/13/17	71	9.5	29.2	35.3	92.1	2.8	0	27.0
MUC 4	7/13/17	71	11.0	12.3	46.8	73.6	3.3	2.1	155.4
MUC 5	7/13/17	319	supernatant	0.0	3.2	0.0	2.4	0	27.4
MUC 5	7/13/17	319	0.5	57.8	30.8	16.6	2.8	4.3	27.2
MUC 5	7/13/17	319	1.5	91.3	52.6	29.4	2.9	3.0	27.1
MUC 5	7/13/17	319	2.5	106.3	55.2	39.1	2.9	3.4	27.1
MUC 5	7/13/17	319	3.5	100.7	58.7	45.6	3.0	3.1	27.0
MUC 5	7/13/17	319	4.5	108.6	54.5	51.4	3.1	2.8	27.0
MUC 5	7/13/17	319	5.5	85.3	45.9	38.3	3.2	3.0	27.0
MUC 5	7/13/17	319	6.5	50.7	37.3	53.0	3.2	2.4	27.1
MUC 5	7/13/17	319	7.5	47.2	25.7	35.6	3.2	0	27.1
MUC 5	7/13/17	319	8.5	32.4	19.7	38.3	3.2	0	-
MUC 5	7/13/17	319	9.5	17.6	16.7	48.0	3.2	0	27.1
MUC 5	7/13/17	319	11.0	13.2	23.3	42.2	3.4	2.1	27.2
MUC 5	7/13/17	319	13.0	9.1	17.2	31.0	3.0	0	27.2
MUC 5	7/13/17	319	15.0	5.6	16.7	32.5	3.1	0	27.0
MUC 6	7/13/17	485	supernatant	0.0	3.7	0.0	2.4	0	27.4
MUC 6	7/13/17	485	0.5	24.5	21.3	2.3	2.6	3.1	27.4
MUC 6	7/13/17	485	1.5	69.8	45.2	13.9	2.9	4.4	27.4
MUC 6	7/13/17	485	2.5	75.1	48.1	19.7	2.7	4.0	-
MUC 6	7/13/17	485	3.5	59.3	31.5	21.7	2.7	3.6	27.5
MUC 6	7/13/17	485	4.5	52.6	27.9	18.6	2.6	3.1	27.4
MUC 6	7/13/17	485	5.5	44.0	29.6	18.6	2.6	2.5	27.4
MUC 6	7/13/17	485	6.5	44.5	26.4	24.8	2.7	2.5	27.5
MUC 6	7/13/17	485	7.5	37.6	23.1	18.6	2.8	3.0	27.5

MUC 6	7/13/17	485	8.5	31.4	22.6	18.2	2.8	2.6	27.5
MUC 6	7/13/17	485	9.5	29.5	19.9	19.0	2.8	2.5	27.5
MUC 6	7/13/17	485	11.0	24.3	18.9	19.0	2.8	0	27.5
MUC 6	7/13/17	485	13.0	17.2	17.4	22.4	2.8	0	27.4
MUC 6	7/13/17	485	15.0	13.1	16.0	20.9	2.7	0	27.5
MUC 6	7/13/17	485	17.0	8.6	16.7	27.9	2.7	0	27.4
MUC 6	7/13/17	485	19.0	8.4	17.1	25.9	2.8	0	27.4
MUC 6	7/13/17	485	22.0	4.1	14.8	22.1	2.8	0	-
MUC 7	7/21/17	537	supernatant	0.0	3.0	0.0	2.4	0	28.0
MUC 7	7/21/17	537	0.5	36.8	21.1	10.2	2.5	3.9	-
MUC 7	7/21/17	537	1.5	114.6	53.4	26.2	2.7	3.7	27.6
MUC 7	7/21/17	537	2.5	127.7	60.0	34.6	2.7	3.1	28.2
MUC 7	7/21/17	537	3.5	129.2	53.6	48.7	2.8	3.0	27.9
MUC 7	7/21/17	537	4.5	125.8	45.7	57.4	2.8	3.1	27.7
MUC 7	7/21/17	537	5.5	114.2	54.2	58.6	2.9	3.2	27.7
MUC 7	7/21/17	537	6.5	99.2	46.3	72.7	3.0	3.1	27.6
MUC 7	7/21/17	537	7.5	89.4	43.7	74.2	3.1	2.8	28.2
MUC 7	7/21/17	537	8.5	86.6	45.1	73.1	3.2	3.0	27.6
MUC 7	7/21/17	537	9.5	71.4	40.2	78.4	3.2	2.1	27.7
MUC 7	7/21/17	537	11.0	60.7	40.3	84.1	3.3	2.4	27.4
MUC 7	7/21/17	537	13.0	46.0	36.8	80.3	3.4	2.1	27.5
MUC 7	7/21/17	537	15.0	39.6	37.6	88.3	3.4	2.1	27.7
MUC 7	7/21/17	537	17.0	34.8	38.3	83.3	3.4	2.8	-
MUC 7	7/21/17	537	19.0	32.9	37.2	91.4	3.4	2.1	27.4
MUC 7	7/21/17	537	22.0	32.1	37.4	75.7	3.4	0	27.5
MUC 8	7/21/17	695	supernatant	0.3	4.0	0.0	2.4	0	28.1
MUC 8	7/21/17	695	0.5	29.5	22.6	4.4	2.5	2.7	27.2
MUC 8	7/21/17	695	1.5	125.8	97.7	11.7	2.5	2.5	27.3
MUC 8	7/21/17	695	2.5	136.0	107.0	22.0	2.5	2.1	27.7
MUC 8	7/21/17	695	3.5	139.0	103.8	29.2	2.5	2.4	27.6
MUC 8	7/21/17	695	4.5	138.2	98.8	34.2	2.5	2.8	27.6
MUC 8	7/21/17	695	5.5	137.8	80.8	34.2	2.5	3.1	27.3
MUC 8	7/21/17	695	6.5	139.7	68.6	33.0	2.7	4.8	27.4
MUC 8	7/21/17	695	7.5	138.2	66.0	36.1	2.7	4.4	27.6
MUC 8	7/21/17	695	8.5	137.8	62.5	35.7	2.8	3.3	28.0
MUC 8	7/21/17	695	9.5	130.0	38.4	31.1	2.9	2.4	27.2
MUC 8	7/21/17	695	11.0	134.1	54.0	34.6	2.9	2.7	27.7
MUC 8	7/21/17	695	13.0	133.0	50.9	38.4	2.9	2.7	27.5
MUC 8	7/21/17	695	15.0	134.5	56.1	44.8	3.0	3.1	26.8
MUC 8	7/21/17	695	17.0	131.1	63.8	49.8	3.1	3.2	27.5
MUC 8	7/21/17	695	19.0	120.6	63.8	60.9	3.2	2.1	27.5
MUC 8	7/21/17	695	22.0	108.2	56.1	67.3	3.2	2.1	27.8
MUC 8	7/21/17	695	26.0	89.0	49.2	71.9	3.3	2.1	-
MUC 8	7/21/17	695	30.0	95.4	55.5	93.3	3.5	0	27.3
MUC 9	7/21/17	907	supernatant	0.9	5.4	0.0	2.4	44.9	27.7

MUC 9	7/21/17	907	0.5	131.1	81.0	28.8	2.6	4.4	27.8
MUC 9	7/21/17	907	1.5	132.2	71.7	49.4	2.9	3.9	27.5
MUC 9	7/21/17	907	2.5	132.2	74.7	67.0	3.0	4.4	27.4
MUC 9	7/21/17	907	3.5	125.8	72.8	87.9	3.3	3.0	26.8
MUC 9	7/21/17	907	4.5	119.8	93.7	99.4	3.4	2.7	27.5
MUC 9	7/21/17	907	5.5	129.6	91.3	107.7	3.6	3.1	26.7
MUC 9	7/21/17	907	6.5	127.3	95.8	138.2	3.8	2.8	26.6
MUC 9	7/21/17	907	7.5	129.6	89.9	154.2	4.0	3.7	26.4
MUC 9	7/21/17	907	8.5	119.8	102.4	165.3	4.1	3.4	26.7
MUC 9	7/21/17	907	9.5	116.8	100.2	176.4	4.2	3.0	26.3
MUC 9	7/21/17	907	11.0	114.9	112.2	183.2	4.4	3.1	26.4
MUC 9	7/21/17	907	13.0	119.5	126.5	205.7	4.7	2.8	26.3
MUC 9	7/21/17	907	15.0	116.1	126.0	219.4	4.9	2.5	26.0
MUC 9	7/21/17	907	17.0	116.4	130.5	229.7	5.1	2.8	26.0
MUC 9	7/21/17	907	19.0	121.7	128.1	259.5	5.4	3.0	25.6
MUC 9	7/21/17	907	22.0	102.2	127.2	281.2	5.9	2.4	25.2
MUC 9	7/21/17	907	26.0	81.1	146.9	327.7	6.4	2.5	24.9
MUC 9	7/21/17	907	30.0	99.6	146.4	412.7	7.2	3.1	24.8
MUC 10	7/27/17	893	supernatant	0.3	4.6	0.0	2.4	0	27.0
MUC 10	7/27/17	893	0.5	155.9	66.2	24.3	2.5	2.8	27.9
MUC 10	7/27/17	893	1.5	175.4	68.1	34.0	2.6	3.7	27.7
MUC 10	7/27/17	893	2.5	154.4	59.2	45.9	2.7	4.2	27.7
MUC 10	7/27/17	893	3.5	170.1	78.0	72.8	2.8	5.2	27.4
MUC 10	7/27/17	893	4.5	173.1	76.6	71.7	2.9	3.6	27.6
MUC 10	7/27/17	893	5.5	158.1	75.2	80.5	3.0	2.6	27.4
MUC 10	7/27/17	893	6.5	171.6	88.8	101.3	3.1	3.4	27.3
MUC 10	7/27/17	893	7.5	153.6	85.0	117.1	3.2	3.4	27.0
MUC 10	7/27/17	893	8.5	137.9	80.3	129.0	3.3	3.2	27.3
MUC 10	7/27/17	893	9.5	133.4	83.6	138.2	3.4	3.3	27.1
MUC 10	7/27/17	893	11.0	143.1	89.2	151.3	3.6	3.4	27.0
MUC 10	7/27/17	893	13.0	138.6	100.0	160.2	3.8	3.1	27.2
MUC 10	7/27/17	893	15.0	117.7	113.6	164.0	3.8	2.7	27.0
MUC 10	7/27/17	893	17.0	95.9	110.4	217.9	4.0	2.8	27.3
MUC 10	7/27/17	893	19.0	107.9	123.5	231.7	4.3	3.1	26.5
MUC 10	7/27/17	893	22.0	115.4	124.0	242.5	4.6	2.7	26.2
MUC 10	7/27/17	893	26.0	59.2	130.1	271.0	5.0	2.1	26.1
MUC 10	7/27/17	893	30.0	47.2	124.9	289.4	5.5	2.2	25.9
MUC 11	7/27/17	745	supernatant	0.0	3.9	0.0	2.3	0	27.8
MUC 11	7/27/17	745	0.5	4.9	22.5	5.9	2.6	3.7	27.6
MUC 11	7/27/17	745	1.5	41.2	44.0	16.3	2.6	3.3	27.7
MUC 11	7/27/17	745	2.5	57.1	44.0	22.4	2.6	0	-
MUC 11	7/27/17	745	3.5	64.8	46.7	28.6	2.8	2.6	27.5
MUC 11	7/27/17	745	4.5	75.3	72.3	36.3	2.8	2.2	27.6
MUC 11	7/27/17	745	5.5	77.0	73.7	49.4	2.9	2.6	28.1
MUC 11	7/27/17	745	6.5	79.4	71.4	50.5	2.9	2.7	29.0

MUC 11	7/27/17	745	7.5	80.5	73.0	64.7	2.9	2.4	27.2
MUC 11	7/27/17	745	8.5	86.7	72.8	72.1	3.0	2.7	27.8
MUC 11	7/27/17	745	9.5	82.6	67.4	73.2	3.1	3.1	28.3
MUC 11	7/27/17	745	11.0	71.4	55.9	75.9	3.1	2.4	27.3
MUC 11	7/27/17	745	13.0	76.8	54.9	79.0	3.1	2.6	27.5
MUC 11	7/27/17	745	15.0	74.0	55.9	87.1	3.2	2.4	27.5
MUC 11	7/27/17	745	17.0	78.3	52.1	81.3	3.2	2.2	27.3
MUC 11	7/27/17	745	19.0	72.9	46.8	90.1	3.1	2.7	27.7
MUC 11	7/27/17	745	22.0	49.1	37.6	84.8	3.2	0	28.0
MUC 11	7/27/17	745	26.0	46.5	37.6	115.1	3.4	0	-
MUC 11	7/27/17	745	30.0	37.7	48.8	96.3	3.4	0	26.9
MUC 12	7/27/17	508	supernatant	0.0	3.5	-	2.3	0	28.0
MUC 12	7/27/17	508	0.5	12.0	16.1	5.9	2.6	3.8	27.7
MUC 12	7/27/17	508	1.5	33.9	38.6	11.3	2.6	3.4	27.9
MUC 12	7/27/17	508	2.5	34.7	38.0	13.6	2.6	3.3	27.9
MUC 12	7/27/17	508	3.5	35.4	34.7	14.7	2.6	3.3	27.7
MUC 12	7/27/17	508	4.5	32.2	31.1	15.5	2.8	3.2	28.2
MUC 12	7/27/17	508	5.5	32.0	32.9	14.7	2.7	3.1	27.9
MUC 12	7/27/17	508	6.5	27.0	22.3	15.1	2.5	2.7	28.0
MUC 12	7/27/17	508	7.5	27.7	20.3	16.7	2.6	2.6	27.7
MUC 12	7/27/17	508	8.5	24.7	17.3	10.5	2.5	2.0	27.6
MUC 12	7/27/17	508	9.5	20.4	15.3	6.6	2.5	2.2	27.3
MUC 12	7/27/17	508	11.0	12.6	11.2	5.1	2.4	0	27.8
MUC 12	7/27/17	508	13.0	6.2	9.8	4.0	2.5	2.5	27.3
MUC 12	7/27/17	508	15.0	5.4	9.8	6.3	2.6	0	29.4
MUC 12	7/27/17	508	17.0	8.1	10.2	12.8	2.5	0	27.9
MUC 12	7/27/17	508	19.0	12.9	11.9	23.6	2.5	0	27.4
MUC 12	7/27/17	508	22.0	7.1	10.8	26.7	2.6	0	28.2

5.1 Instrumental nitrate errors

Porewater NO_3^- data of the present study, even though an integral part of redox interpretations, were questionable. In the sediment, we would expect to see a peak in NO_3^- at the top of the core before a peak in sulfate reduction and iron reduction, since NO_3^- has the second highest Gibbs free energy gain, following O_2 (Jørgensen, 2006). Moving down core, we would expect to see very little to zero NO_3 (µM). In all cores, porewater NO_3^- neither peaked nor declined to 0 µM NO_3^-. Moreover, porewater concentrations of NO_3^- centered around one number for the cores that were grouped on the same run (Table 5-2). The NO_3^- standards were recovered both at the start and end

of every analytical run, suggesting that the ion chromatograph was functioning properly. More detailed analyses on detection limits and filtering of samples for the ion chromatograph are necessary for moving forward on NO_3^-. Otherwise, a different technique, such as the flow injection analyzer method (Hofer, 2003; Knepel, 2003) or the reduction of NO_3^- by shaking with cadmium method (Jones, 1983) should be explored. I could not perform the flow injection type of analysis as part of my research as this technique requires at least 4 mL and less than 1 mL remained from my samples. Most samples contained 0 mL porewater after all of the analyses were complete. The shaking with cadmium method only requires 500 µL of sample, but I was not able to use this method from lack of time to complete the analyses before my thesis deadline.

Table 5-2: Nitrate data for MUCs 1-12. Nitrate (µM) was measured on the ion chromatograph. Run A: MUCs 1,2,4,7; RUN B: MUC 3; RUN C: MUCs 5,6; RUN D: MUCs 8,9; RUN E: MUCS 10,11,12.

Core ID	Water depth (m)	Sediment depth (cm)	Nitrate (µM)
MUC 1	154	supernatant	37.6
MUC 1	154	0.5	7.6
MUC 1	154	1.5	7.3
MUC 1	154	2.5	-
MUC 1	154	3.5	22.0
MUC 1	154	4.5	-
MUC 1	154	5.5	-
MUC 1	154	6.5	-
MUC 1	154	7.5	-
MUC 1	154	8.5	-
MUC 1	154	9.5	-
MUC 1	154	11.0	4.8
MUC 1	154	13.0	5.8
MUC 2	399	supernatant	45.3
MUC 2	399	0.5	14.8
MUC 2	399	1.5	10.4
MUC 2	399	2.5	10.5
MUC 2	399	3.5	9.9
MUC 2	399	4.5	11.9

MUC 2	399	5.5	11.2
MUC 2	399	6.5	13.5
MUC 2	399	7.5	13.5
MUC 2	399	8.5	9.9
MUC 2	399	9.5	-
MUC 2	399	11.0	12.7
MUC 2	399	13.0	10.8
MUC 2	399	15.0	11.4
MUC 2	399	17.0	11.2
MUC 3	777	supernatant	44.6
MUC 3	777	0.5	3.7
MUC 3	777	1.5	2.0
MUC 3	777	2.5	5.4
MUC 3	777	3.5	5.5
MUC 3	777	4.5	1.8
MUC 3	777	5.5	2.8
MUC 3	777	6.5	3.1
MUC 3	777	7.5	2.5
MUC 3	777	8.5	3.6
MUC 3	777	9.5	2.0
MUC 3	777	11.0	4.0
MUC 3	777	13.0	3.1
MUC 3	777	15.0	3.7
MUC 3	777	17.0	2.7
MUC 3	777	19.0	2.1
MUC 3	777	22.0	2.2
MUC 3	777	26.0	1.9
MUC 3	777	30.0	0.0
MUC 4	71	supernatant	37.6
MUC 4	71	0.5	10.0
MUC 4	71	1.5	7.3
MUC 4	71	2.5	5.4
MUC 4	71	3.5	-
MUC 4	71	4.5	-
MUC 4	71	5.5	-
MUC 4	71	6.5	-
MUC 4	71	7.5	-
MUC 4	71	8.5	-
MUC 4	71	9.5	-
MUC 4	71	11.0	-
MUC 5	319	supernatant	7.6
MUC 5	319	0.5	2.4
MUC 5	319	1.5	3.1

MUC 5	319	2.5	1.5
MUC 5	319	3.5	14.2
MUC 5	319	4.5	0.2
MUC 5	319	5.5	2.8
MUC 5	319	6.5	5.9
MUC 5	319	7.5	3.0
MUC 5	319	8.5	0.9
MUC 5	319	9.5	-
MUC 5	319	11.0	-
MUC 5	319	13.0	-
MUC 5	319	15.0	-
MUC 6	485	supernatant	42.4
MUC 6	485	0.5	3.5
MUC 6	485	1.5	2.9
MUC 6	485	2.5	1.8
MUC 6	485	3.5	2.0
MUC 6	485	4.5	3.6
MUC 6	485	5.5	1.7
MUC 6	485	6.5	2.4
MUC 6	485	7.5	2.6
MUC 6	485	8.5	2.9
MUC 6	485	9.5	1.5
MUC 6	485	11.0	19.4
MUC 6	485	13.0	3.3
MUC 6	485	15.0	3.0
MUC 6	485	17.0	2.8
MUC 6	485	19.0	3.2
MUC 6	485	22.0	1.5
MUC 7	537	supernatant	48.2
MUC 7	537	0.5	14.9
MUC 7	537	1.5	9.0
MUC 7	537	2.5	8.2
MUC 7	537	3.5	9.1
MUC 7	537	4.5	8.7
MUC 7	537	5.5	10.1
MUC 7	537	6.5	8.8
MUC 7	537	7.5	9.9
MUC 7	537	8.5	10.5
MUC 7	537	9.5	8.3
MUC 7	537	11.0	8.0
MUC 7	537	13.0	9.7
MUC 7	537	15.0	12.8
MUC 7	537	17.0	8.9

MUC 7	537	19.0	8.1
MUC 7	537	22.0	9.3
MUC 8	695	supernatant	37.4
MUC 8	695	0.5	4.9
MUC 8	695	1.5	6.9
MUC 8	695	2.5	7.4
MUC 8	695	3.5	8.2
MUC 8	695	4.5	4.4
MUC 8	695	5.5	6.3
MUC 8	695	6.5	6.3
MUC 8	695	7.5	6.9
MUC 8	695	8.5	6.2
MUC 8	695	9.5	6.0
MUC 8	695	11.0	8.1
MUC 8	695	13.0	5.8
MUC 8	695	15.0	7.6
MUC 8	695	17.0	8.4
MUC 8	695	19.0	7.1
MUC 8	695	22.0	5.1
MUC 8	695	26.0	6.2
MUC 8	695	30.0	7.1
MUC 9	907	supernatant	32.7
MUC 9	907	0.5	6.7
MUC 9	907	1.5	7.7
MUC 9	907	2.5	7.1
MUC 9	907	3.5	5.7
MUC 9	907	4.5	5.8
MUC 9	907	5.5	7.1
MUC 9	907	6.5	17.2
MUC 9	907	7.5	6.1
MUC 9	907	8.5	7.9
MUC 9	907	9.5	7.3
MUC 9	907	11.0	7.6
MUC 9	907	13.0	5.3
MUC 9	907	15.0	6.8
MUC 9	907	17.0	6.5
MUC 9	907	19.0	7.1
MUC 9	907	22.0	5.4
MUC 9	907	26.0	7.4
MUC 9	907	30.0	7.7
MUC 10	893	supernatant	73.8
MUC 10	893	0.5	26.7
MUC 10	893	1.5	0.1

MUC 10	893	2.5	38.2
MUC 10	893	3.5	33.8
MUC 10	893	4.5	34.8
MUC 10	893	5.5	31.8
MUC 10	893	6.5	41.5
MUC 10	893	7.5	36.0
MUC 10	893	8.5	35.6
MUC 10	893	9.5	39.5
MUC 10	893	11.0	34.7
MUC 10	893	13.0	30.9
MUC 10	893	15.0	44.6
MUC 10	893	17.0	41.0
MUC 10	893	19.0	38.0
MUC 10	893	22.0	41.5
MUC 10	893	26.0	0.1
MUC 10	893	30.0	34.2
MUC 11	745	supernatant	75.4
MUC 11	745	0.5	33.3
MUC 11	745	1.5	36.4
MUC 11	745	2.5	36.1
MUC 11	745	3.5	40.2
MUC 11	745	4.5	30.5
MUC 11	745	5.5	34.0
MUC 11	745	6.5	33.3
MUC 11	745	7.5	40.0
MUC 11	745	8.5	42.4
MUC 11	745	9.5	35.9
MUC 11	745	11.0	32.3
MUC 11	745	13.0	36.4
MUC 11	745	15.0	32.5
MUC 11	745	17.0	31.0
MUC 11	745	19.0	40.4
MUC 11	745	22.0	34.6
MUC 11	745	26.0	32.6
MUC 11	745	30.0	32.6
MUC 12	508	supernatant	53.2
MUC 12	508	0.5	19.9
MUC 12	508	1.5	20.7
MUC 12	508	2.5	19.1
MUC 12	508	3.5	20.8
MUC 12	508	4.5	20.7
MUC 12	508	5.5	19.0
MUC 12	508	6.5	24.4

MUC 12	508	7.5	19.2
MUC 12	508	8.5	20.8
MUC 12	508	9.5	18.8
MUC 12	508	11.0	19.1
MUC 12	508	13.0	21.5
MUC 12	508	15.0	20.3
MUC 12	508	17.0	22.9
MUC 12	508	19.0	18.5
MUC 12	508	22.0	13.0

Table 5-3: Sulfate reduction (nmol cm^3 d^{-1}) *MUC 1-3 replicates.

Core ID	Water depth (m)	Sediment depth (cm)	SR (nmol cm^3 d^{-1})
MUC 1	154	0.5	6.1
MUC 1	154	1.5	8.9
MUC 1	154	2.5	5.8
MUC 1	154	3.5	10.0
MUC 1	154	4.5	9.4
*MUC 1	154	0.5	1.1
*MUC 1	154	1.5	19.1
*MUC 1	154	2.5	62.3
*MUC 1	154	3.5	38.3
*MUC 1	154	4.5	11.0
MUC 2	399	0.5	7.3
MUC 2	399	1.5	10.9
MUC 2	399	2.5	6.9
MUC 2	399	3.5	13.5
MUC 2	399	4.5	12.3
MUC 2	399	5.5	12.7
MUC 2	399	6.5	17.6
MUC 2	399	7.5	10.8
MUC 2	399	8.5	5.9
*MUC 2	399	0.5	6.2
*MUC 2	399	1.5	9.7
*MUC 2	399	2.5	12.3
*MUC 2	399	3.5	5.6
*MUC 2	399	4.5	11.3
*MUC 2	399	5.5	7.1
*MUC 2	399	6.5	9.9
*MUC 2	399	7.5	2.8
*MUC 2	399	8.5	6.9

*MUC 2	399	9.5	-
*MUC 2	399	10.5	7.7
*MUC 2	399	11.5	13.1
*MUC 2	399	12.5	12.3
*MUC 2	399	13.5	6.3
*MUC 2	399	14.5	12.1
*MUC 2	399	15.5	7.0
*MUC 2	399	16.5	13.1
*MUC 2	399	17.5	9.1
MUC 3	777	0.5	8.2
MUC 3	777	1.5	17.3
MUC 3	777	2.5	4.2
MUC 3	777	3.5	4.4
MUC 3	777	4.5	4.9
MUC 3	777	5.5	-
MUC 3	777	6.5	5.1
MUC 3	777	7.5	10.1
MUC 3	777	8.5	6.1
MUC 3	777	9.5	3.9
MUC 3	777	10.5	3.3
MUC 3	777	11.5	3.8
MUC 3	777	12.5	3.1
MUC 3	777	13.5	2.2
MUC 3	777	14.5	2.1
MUC 3	777	15.5	2.6
MUC 3	777	16.5	4.2
MUC 3	777	17.5	2.2
MUC 3	777	18.5	2.4
MUC 3	777	19.5	1.7
*MUC 3	777	0.5	16.7
*MUC 3	777	1.5	14.5
*MUC 3	777	2.5	9.9
*MUC 3	777	3.5	9.0
*MUC 3	777	4.5	5.1
*MUC 3	777	5.5	-
*MUC 3	777	6.5	4.1
*MUC 3	777	7.5	3.9
*MUC 3	777	8.5	3.3
*MUC 3	777	9.5	3.3
*MUC 3	777	10.5	2.5
*MUC 3	777	11.5	2.5
*MUC 3	777	12.5	3.2
*MUC 3	777	13.5	2.9

*MUC 3	777	14.5	2.3
*MUC 3	777	15.5	2.7
*MUC 3	777	16.5	1.5
*MUC 3	777	17.5	2.4
*MUC 3	777	18.5	2.3
*MUC 3	777	19.5	1.9
*MUC 3	777	20.5	2.0
MUC 4	71	0.5	0.2
MUC 4	71	1.5	0.2
MUC 4	71	2.5	0.4
MUC 4	71	3.5	4.7
MUC 4	71	4.5	6.5
MUC 4	71	5.5	3.2
MUC 4	71	6.5	-
MUC 4	71	7.5	4.2
MUC 4	71	8.5	2.0
MUC 5	319	0.5	11.1
MUC 5	319	1.5	2.5
MUC 5	319	2.5	3.1
MUC 5	319	3.5	3.5
MUC 5	319	4.5	0.8
MUC 5	319	5.5	6.6
MUC 5	319	6.5	4.5
MUC 5	319	7.5	6.9
MUC 5	319	8.5	-
MUC 5	319	9.5	7.4
MUC 5	319	10.5	5.0
MUC 5	319	11.5	7.4
MUC 5	319	12.5	3.9
MUC 5	319	13.5	4.3
MUC 6	485	0.5	7.3
MUC 6	485	1.5	6.6
MUC 6	485	2.5	-
MUC 6	485	3.5	7.7
MUC 6	485	4.5	7.5
MUC 6	485	5.5	3.2
MUC 6	485	6.5	3.1
MUC 6	485	7.5	2.1
MUC 6	485	8.5	2.4
MUC 6	485	9.5	3.7
MUC 6	485	10.5	1.6
MUC 6	485	11.5	4.4
MUC 6	485	12.5	2.3

MUC 7	537	0.5	-
MUC 7	537	1.5	3.5
MUC 7	537	2.5	2.9
MUC 7	537	3.5	3.6
MUC 7	537	4.5	2.8
MUC 7	537	5.5	3.4
MUC 7	537	6.5	1.0
MUC 7	537	7.5	6.3
MUC 7	537	8.5	3.3
MUC 7	537	9.5	1.3
MUC 7	537	10.5	3.5
MUC 7	537	11.5	2.1
MUC 7	537	12.5	3.0
MUC 7	537	13.5	2.1
MUC 7	537	14.5	2.6
MUC 7	537	15.5	1.2
MUC 7	537	16.5	0.0
MUC 7	537	17.5	0.0
MUC 7	537	18.5	1.9
MUC 7	537	19.5	1.2
MUC 7	537	20.5	1.5
MUC 7	537	21.5	1.1
MUC 7	537	22.5	0.5
MUC 8	695	0.5	0.7
MUC 8	695	1.5	3.0
MUC 8	695	2.5	3.7
MUC 8	695	3.5	1.5
MUC 8	695	4.5	1.1
MUC 8	695	5.5	2.4
MUC 8	695	6.5	2.3
MUC 8	695	7.5	4.2
MUC 8	695	8.5	2.6
MUC 8	695	9.5	4.7
MUC 8	695	10.5	3.7
MUC 8	695	11.5	6.0
MUC 8	695	12.5	4.3
MUC 8	695	13.5	5.7
MUC 8	695	14.5	5.9
MUC 8	695	15.5	2.8
MUC 8	695	16.5	5.2
MUC 8	695	17.5	4.8
MUC 8	695	18.5	4.3
MUC 8	695	19.5	3.2

MUC 8	695	20.5	4.1
MUC 8	695	21.5	2.5
MUC 8	695	22.5	2.7
MUC 8	695	23.5	1.8
MUC 9	907	0.5	15.7
MUC 9	907	1.5	5.4
MUC 9	907	2.5	7.6
MUC 9	907	3.5	6.0
MUC 9	907	4.5	4.6
MUC 9	907	5.5	3.5
MUC 9	907	6.5	4.6
MUC 9	907	7.5	3.5
MUC 9	907	8.5	1.1
MUC 9	907	9.5	2.5
MUC 9	907	10.5	2.4
MUC 9	907	11.5	2.3
MUC 9	907	12.5	2.5
MUC 9	907	13.5	2.2
MUC 9	907	14.5	2.0
MUC 9	907	15.5	1.5
MUC 9	907	16.5	1.7
MUC 9	907	17.5	1.1
MUC 9	907	18.5	1.6
MUC 9	907	19.5	1.5
MUC 9	907	20.5	1.6
MUC 9	907	21.5	1.3
MUC 9	907	22.5	1.3
MUC 9	907	23.5	0.9
MUC 9	907	24.5	1.3
MUC 10	893	0.5	11.3
MUC 10	893	1.5	8.5
MUC 10	893	2.5	5.1
MUC 10	893	3.5	3.9
MUC 10	893	4.5	2.6
MUC 10	893	5.5	2.0
MUC 10	893	6.5	3.7
MUC 10	893	7.5	4.7
MUC 10	893	8.5	5.1
MUC 10	893	9.5	2.9
MUC 10	893	10.5	3.3
MUC 10	893	11.5	3.3
MUC 10	893	12.5	1.2
MUC 10	893	13.5	1.0

MUC 10	893	14.5	1.3
MUC 10	893	15.5	0.8
MUC 10	893	16.5	1.1
MUC 10	893	17.5	1.3
MUC 10	893	18.5	1.5
MUC 10	893	19.5	1.7
MUC 10	893	20.5	1.9
MUC 10	893	21.5	1.0
MUC 10	893	22.5	1.0
MUC 10	893	23.5	1.6
MUC 10	893	24.5	2.1
MUC 11	745	0.5	0.2
MUC 11	745	1.5	2.2
MUC 11	745	2.5	0.0
MUC 11	745	3.5	0.4
MUC 11	745	4.5	1.9
MUC 11	745	5.5	2.7
MUC 11	745	6.5	3.0
MUC 11	745	7.5	2.9
MUC 11	745	8.5	2.1
MUC 11	745	9.5	3.4
MUC 11	745	10.5	4.2
MUC 11	745	11.5	4.0
MUC 11	745	12.5	4.0
MUC 11	745	13.5	4.8
MUC 11	745	14.5	3.5
MUC 11	745	15.5	4.3
MUC 11	745	16.5	4.5
MUC 11	745	17.5	3.4
MUC 11	745	18.5	3.6
MUC 11	745	19.5	2.8
MUC 11	745	20.5	1.9
MUC 11	745	21.5	1.6
MUC 11	745	22.5	1.5
MUC 11	745	23.5	0.9
MUC 12	508	0.5	0.3
MUC 12	508	1.5	2.3
MUC 12	508	2.5	1.8
MUC 12	508	3.5	1.6
MUC 12	508	4.5	1.1
MUC 12	508	5.5	2.6
MUC 12	508	6.5	0.8
MUC 12	508	7.5	1.4

MUC 12	508	8.5	0.1
MUC 12	508	9.5	1.3
MUC 12	508	10.5	1.1
MUC 12	508	11.5	1.1
MUC 12	508	12.5	0.5
MUC 12	508	13.5	0.4
MUC 12	508	14.5	0.3
MUC 12	508	15.5	0.3
MUC 12	508	16.5	0.1
MUC 12	508	17.5	0.2
MUC 12	508	18.5	0.8
MUC 12	508	19.5	0.4
MUC 12	508	20.5	0.6
MUC 12	508	21.5	0.4

Table 5-4. Integrated sulfate reduction (mmol m^{-2} d^{-1}). Rates were integrated over the top 10 cm of core depth for all stations except MUC 1 and MUC 4, stations that only had 5 and 9 cm of samples, respectively.

Core ID	Water depth (m)	Integrated SR (mmol m^{-2} d^{-1})	Integration depth (cm)
MUC 1	154	0.86	5
MUC 2	399	0.85	10
MUC 3	777	0.67	10
MUC 4	71	0.21	9
MUC 5	319	0.46	10
MUC 6	485	0.44	10
MUC 7	537	0.28	10
MUC 8	695	0.26	10
MUC 9	907	0.55	10
MUC 10	893	0.50	10
MUC 11	745	0.19	10
MUC 12	508	0.13	10

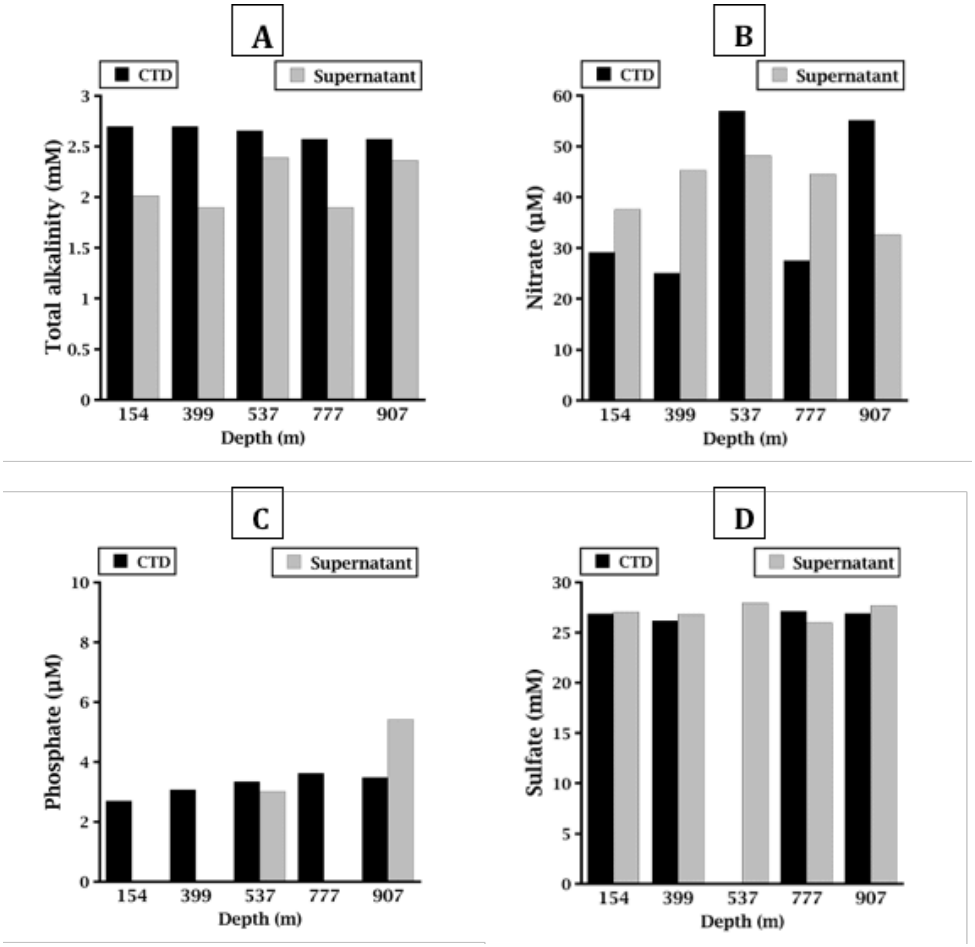

Figure 5-1: CTD bottom water vs. core supernatant water. Concentrations of total alkalinity (A, mM), Nitrate (B, µM), Phosphate (C, mM), and Sulfate (D, mM) from the five CTD cast stations and corresponding MUC cores (154, 319, 399, 777 and 907 m water depths).

Table 5-5: Porosity. Porosity data for each MUC.

MUC ID	Water depth (m)	Sediment depth (cm)	Porosity
1	154	0.5	0.606
1	154	1.5	0.591
1	154	2.5	0.574
1	154	3.5	0.570
1	154	4.5	0.577
2	399	0.5	0.772
2	399	1.5	0.749
2	399	2.5	0.742
2	399	3.5	0.723
2	399	4.5	0.719

2	399	5.5	0.705
2	399	6.5	0.684
2	399	7.5	0.651
2	399	8.5	0.656
2	399	9.5	0.660
2	399	11	0.644
2	399	13	0.600
2	399	15	0.618
2	399	17	0.641
2	399	19	0.636
3	777	0.5	0.899
3	777	1.5	0.870
3	777	2.5	0.874
3	777	3.5	0.867
3	777	4.5	0.838
3	777	5.5	0.797
3	777	6.5	0.796
3	777	7.5	0.783
3	777	8.5	0.781
3	777	9.5	0.779
3	777	11	0.776
3	777	13	0.764
3	777	15	0.777
3	777	17	0.770
3	777	19	0.774
4	71	0.5	0.643
4	71	1.5	0.595
4	71	2.5	0.575
4	71	3.5	0.566
4	71	4.5	0.559
4	71	6	0.527
4	71	8	0.524
5	319	0.5	0.764
5	319	1.5	0.736
5	319	2.5	0.740
5	319	3.5	0.707
5	319	4.5	0.700
5	319	6	0.703
5	319	8	0.680
5	319	10	0.673
5	319	12	0.651
5	319	13.5	0.616

6	485	0.5	0.859
6	485	1.5	0.812
6	485	2.5	0.802
6	485	3.5	0.789
6	485	4.5	0.781
6	485	6	0.764
6	485	8	0.726
6	485	10	0.721
6	485	12	0.715
6	485	14	0.717
6	485	16	0.703
6	485	18	0.708
6	485	20	0.699
6	485	26	0.664
7	537	0.5	0.767
7	537	1.5	0.720
7	537	2.5	0.713
7	537	3.5	0.716
7	537	4.5	0.731
7	537	5.5	0.710
7	537	6.5	0.695
7	537	8	0.691
7	537	10	0.698
7	537	12	0.669
7	537	14	0.664
7	537	16	0.651
7	537	18	0.644
7	537	20	0.629
7	537	22	0.633
8	695	0.5	0.839
8	695	1.5	0.824
8	695	2.5	0.875
8	695	3.5	0.826
8	695	4.5	0.806
8	695	5.5	0.801
8	695	6.5	0.785
8	695	8	0.786
8	695	10	0.792
8	695	12	0.799
8	695	14	0.828
8	695	16	0.769
8	695	18	0.763
8	695	20	0.738

8	695	22	0.738
8	695	24	0.743
8	695	26	0.759
8	695	28	0.743
8	695	30	0.729
9	907	0.5	0.921
9	907	1.5	0.895
9	907	2.5	0.902
9	907	3.5	0.887
9	907	4.5	0.870
9	907	5.5	0.870
9	907	6.5	0.861
9	907	8	0.862
9	907	10	0.868
9	907	12	0.865
9	907	14	0.863
9	907	16	0.866
9	907	18	0.853
9	907	20	0.866
9	907	22	0.856
9	907	24	0.824
9	907	26	0.733
9	907	28	0.722
9	907	30	0.706
9	907	32	0.697
10	893	0.5	0.910
10	893	1.5	0.879
10	893	2.5	0.879
10	893	3.5	0.871
10	893	4.5	0.867
10	893	5.5	0.863
10	893	6.5	0.857
10	893	8	0.852
10	893	10	0.857
10	893	12	0.835
10	893	14	0.731
10	893	16	0.680
10	893	18	0.755
10	893	20	0.837
10	893	22	0.773
10	893	24	0.816
10	893	26	0.815
10	893	28	0.748

10	893	30	0.708
11	745	0.5	0.884
11	745	1.5	0.878
11	745	2.5	0.873
11	745	3.5	0.866
11	745	4.5	0.851
11	745	5.5	0.843
11	745	6.5	0.833
11	745	8	0.835
11	745	10	0.868
11	745	12	0.819
11	745	14	0.811
11	745	16	0.807
11	745	18	0.821
11	745	20	0.814
11	745	22	0.815
11	745	24	0.807
11	745	26	0.804
11	745	28	0.789
12	508	0.5	0.844
12	508	1.5	0.776
12	508	2.5	0.634
12	508	3.5	0.770
12	508	4.5	0.730
12	508	5.5	0.705
12	508	6.5	0.705
12	508	8	0.692
12	508	10	0.687
12	508	12	0.682
12	508	14	0.647
12	508	16	0.663
12	508	18	0.655
12	508	20	0.643
12	508	22	0.633

References

Alexander, C.R., Venherm, C., 2003. Modern sedimentary processes in the Santa Monica, California continental margin: Sediment accumulation, mixing and budget. Mar. Environ. Res. doi:10.1016/S0141-1136(02)00330-6

Berelson, W.M., 1991. The Flushing of Two Deep-Sea Basins, Southern California Borderland. Limnol. Oceanogr. 36, 1150–1166. doi:10.4319/lo.1991.36.6.1150

Berelson, W.M., Stott, L.D., 2003. Productivity and organic carbon rain to the California margin seafloor: Modern and paleoceanographic perspectives. Paleoceanography 18, 1–15. doi:10.1029/2001PA000672

Blatt, H., Tracy, R.J., Owens, B.E., 2006. Petrology: igneous, sedimentary, and metamorphic. W.H. Freeman, New York.

Bograd, S.J., Castro, C.G., Di Lorenzo, E., Palacios, D.M., Bailey, H., Gilly, W., Chavez, F.P., 2008. Oxygen declines and the shoaling of the hypoxic boundary in the California Current. Geophys. Res. Lett. doi:10.1029/2008GL034185

Brüchert, V., Jørgensen, B.B., Neumann, K., Riechmann, D., Schlösser, M., Schulz, H., 2003. Regulation of bacterial sulfate reduction and hydrogen sulfide fluxes in the central namibian coastal upwelling zone. Geochimica et Cosmochimica Acta 67, 4505–4518. doi:10.1016/s0016-7037(03)00275-8

Calvert, S.E., 1965. Factors affecting distribution of laminated diatomacous sediments in Gulf of California. Deep Sea Research and Oceanographic Abstracts 12, 572. doi:10.1016/0011-7471(65)90460-2

Canfield, D.E., 1989. Reactive iron in marine sediments. Geochimica et Cosmochimica Acta 53, 619–632. doi:10.1016/0016-7037(89)90005-7

Chavez, F.P., Messié, M., 2009. A comparison of Eastern Boundary Upwelling Ecosystems. Prog. Oceanogr. 83, 80–96. doi:10.1016/j.pocean.2009.07.032

Childress, J.J., Seibel, B.A., 1998. Life at stable low oxygen levels: adaptations of animals to oceanic oxygen minimum layers. J. Exp. Biol. 201.

Christensen, C.J., Gorsline, D.S., Hammond, D.E., Lund, S.P., 1994. Non-annual laminations and expansion of anoxic basin-floor conditions in Santa Monica Basin, California Borderland, over the past four centuries. Mar. Geol. 116, 399–418. doi:10.1016/0025-3227(94)90054-X

Dojiri, M., Yamaguchi, M., Weisberg, S.B., Lee, H.J., 2003. Changing anthropogenic influence on the Santa Monica Bay watershed. Mar. Environ. Res. 56, 1–14. doi:10.1016/S0141-1136(03)00003-5

Elrod, V.A., Berelson, W.M., Coale, K.H., Johnson, K.S., 2004. The flux of iron from continental shelf sediments: A missing source for global budgets. Geophysical Research Letters 31. doi:10.1029/2004gl020216

Ferdelman, T.G., Lee, C., Pantoja, S., Harder, J., Bebout, B.M., Fossing, H., 1997. Sulfate reduction and methanogenesis in a Thioploca-dominated sediment off the coast of Chile. Geochimica et Cosmochimica Acta 61, 3065–3079. doi:10.1016/s0016-7037(97)00158-0

Fossing, H., 1990. Sulfate reduction in shelf sediments in the upwelling region off Central Peru. Continental Shelf Research 10, 355–367. doi:10.1016/0278-4343(90)90056-r

Fossing, H., Ferdelman, T.G., Berg, P., 2000. Sulfate reduction and methane oxidation in continental margin sediments influenced by irrigation (South-East Atlantic off Namibia). Geochimica et Cosmochimica Acta 64, 897–910. doi:10.1016/s0016-7037(99)00349-x

Gong, C., Hollander, D.J., 1997. Differential contribution of bacteria to sedimentary organic matter in oxic and anoxic environments, Santa Monica Basin, California.

Organic Geochemistry 26, 545–563. doi:10.1016/s0146-6380(97)00018-1

Gong, C., Hollander, D.J., 1999. Evidence for differential degradation of alkenones under contrasting bottom water oxygen conditions: implication for paleotemperature reconstruction. Geochimica et Cosmochimica Acta 63, 405–411. doi:10.1016/s0016-7037(98)00283-x

Gorsline, D.S., 1996. Depositional events in Santa Monica Basin, California Borderland, over the past five centuries. Sediment. Geol. Sediment. Geol. Sedimentary Geol. 104, 73–88.

Gorsline, D.S., 1992. The geological setting of Santa Monica and San Pedro Basins, California Continental Borderland. Prog. Oceanogr. 30, 1–36. doi:10.1016/0079-6611(92)90008-N

Grant , 1991. Lateral and Vertical Distributions and Textural Features of Filamentous Bacterial (Beggiatoa sp.) Mats in Santa Barbara Basin, California. AAPG Bulletin 75. doi:10.1306/20b24358-170d-11d7-8645000102c1865d

Ehrhardt, M., Grasshoff, K., Kremling, K., 1998. Methods of seawater analysis. Wiley-VCH, Weinheim.

Gruber, N., Lachkar, Z., Frenzel, H., Marchesiello, P., Münnich, M., McWilliams, J.C., Nagai, T., Plattner, G.-K., 2011. Eddy-induced reduction of biological production in eastern boundary upwelling systems. Nat. Geosci. 4, 787–792. doi:10.1038/ngeo1273

Heintz, M.B., Mau, S., Valentine, D.L., 2012. Physical control on methanotrophic potential in waters of the Santa Monica Basin , Southern California 57, 420–432. doi:10.4319/lo.2012.57.2.0420

Hickey, B.M., 1992. Circulation over the Santa M o n i c a - S a n Pedro Basin and S h e l f 30, 37–115.

Hofer, S. 2003. Determination of Ammonia (Salicylate) in 2M KCl soil extracts by Flow Injection Analysis. QuikChem Method 12-107-06-2-A. Lachat Instruments, Loveland, CO.

Huettel, M., Berg, P., Kostka, J.E., 2014. Benthic Exchange and Biogeochemical Cycling in Permeable Sediments. Annual Review of Marine Science 6, 23–51. doi:10.1146/annurev-marine-051413-012706

Huh, C.A., Small, L.F., Niemnil, S., Finney, B.P., Hickey, B.M., Kachel, N.B., Gorsline, D.S., Williams, P.M., 1990. Sedimentation dynamics in the Santa Monica-San Pedro Basin off Los Angeles: radiochemical, sediment trap and transmissometer studies. Cont. Shelf Res. 10, 137–164. doi:10.1016/0278-4343(90)90027-J

Huyer, A., 1983. Coastal upwelling in the California Current System. Prog. Oceanogr. 12, 259–284. doi:10.1016/0079-6611(83)90010-1

Ivanenkov, V.N., Lyakhin, Y., 1978. Determination of total alkalinity in seawater, in: Methods of hydrochemical investigations in the oceans. pp. 110–114.

Iversen, N., Jørgensen, B.B., 1993. Diffusion coefficients of sulfate and methane in marine sediments: Influence of porosity. Geochimica et Cosmochimica Acta 57, 571–578. doi:10.1016/0016-7037(93)90368-7

Jahnke, R.A., 1990. Early diagenesis and recycling of biogenic debris at the seafloor, Santa Monica Basin, California. Journal of Marine Research 48, 413–436. doi:10.1357/002224090784988773

Jørgensen, B.B., 2000. Bacteria and marine biogeochemistry. In: Schulz HD, Zabel M (eds) Marine biogeochemistry. Springer, Berlin, pp 173–201

Jørgensen, B.B., 2006. Marine Geochemistry. doi:10.1007/3-540-32144-6

Jørgensen, B.B., 1978. A comparison of methods for the quantification of bacterial sulfate reduction in coastal marine sediments: II. calculation from mathematical

models. Geomicrobiol. J. 1, 29–47. doi:10.1080/01490457809377722

Kallmeyer, J., Ferdelman, T.G., Weber, A., Fossing, H., Jørgensen, B.B., 2004. A cold chromium distillation procedure for radiolabeled sulfide applied to sulfate reduction measurements. Limnol. Oceanogr. 2, 171–180. doi:10.4319/lom.2004.2.171

Keeling, R.F., Garcia, H.E., 2002. The change in oceanic O2 inventory associated with recent global warming. Proceedings of the National Academy of Sciences 99, 7848–7853. doi:10.1073/pnas.122154899

Knepel, K. 2003. Determination of Nitrate in 2M KCl soil extracts by Flow Injection Analysis. QuikChem Method 12-107-04-1-B. Lachat Instruments, Loveland, CO.

Komada, T., Burdige, D.J., Crispo, S.M., Druffel, E.R., Griffin, S., Johnson, L., Le, D., 2013. Dissolved organic carbon dynamics in anaerobic sediments of the Santa Monica Basin. Geochimica et Cosmochimica Acta 110, 253–273. doi:10.1016/j.gca.2013.02.017

Komada, T., Burdige, D.J., Magen, C., Li, H.-L., Chanton, J., 2016. Recycling of Organic Matter in the Sediments of Santa Monica Basin, California Borderland. Aquatic Geochemistry 22, 593–618. doi:10.1007/s10498-016-9308-0

Kraal, P., Slomp, C.P., Reed, D.C., Reichart, G.J., Poulton, S.W., 2012. Sedimentary phosphorus and iron cycling in and below the oxygen minimum zone of the northern Arabian Sea. Biogeosciences 9, 2603–2624. doi:10.5194/bg-9-2603-2012

Kristensen, E., Penha-Lopes, G., Delefosse, M., Valdemarsen, T., Quintana, C., Banta, G., 2012. What is bioturbation? The need for a precise definition for fauna in aquatic sciences. Marine Ecology Progress Series 446, 285–302. doi:10.3354/meps09506

Kumar, S., 2007. Fourth assessment report of the Intergovernmental Panel on Climate Change: important observations and conclusions. *Curr. Sci.* **92**, 1034–1034.

Lein, A. Y., Ivonov, M. V., 1990. Production of hydrogen sulfide in shelf sediments and its balance in the Black Sea. Mikrobiologiya, 59.921-928. (English translation)

Lein, A. Y., Ivonov, M. V., Vainshtein, M. B., 1990. Hydrogen sulfide balance in the deep water zone of the Black Sea. Mikrobiologiya, 59,6X1-665. (English translation)

Levin, L.A., 2003. OXYGEN MINIMUM ZONE BENTHOS: ADAPTATION AND COMMUNITY RESPONSE TO HYPOXIA 41, 1–45.

Masiello, C.A., Druffel, E.R.M., 2003. Organic and black carbon13C and14C through the Santa Monica Basin sediment oxic-anoxic transition. Geophysical Research Letters 30. doi:10.1029/2002gl015050

Middelburg, J.J., Levin, L.A., 2009. Coastal hypoxia and sediment biogeochemistry. Biogeosciences 6, 3655–3706. doi:10.5194/bgd-6-3655-2009

Monteverde, D.R., Gómez-Consarnau, L., Cutter, L., Chong, L., Berelson, W., Sañudo-Wilhelmy, S.A., 2015. Vitamin B1 in marine sediments: pore water concentration gradient drives benthic flux with potential biological implications. Frontiers in Microbiology 6. doi:10.3389/fmicb.2015.00434

Nealson, K.H., 1997. Sediment Bacteria: Who' s There, What Are They Doing, and What's New? Annu. Rev. Earth Planet. Sci. 25, 403–434. doi:10.1146/annurev.earth.25.1.403

Paulmier, A., Ruiz-Pino, D., 2009. Oxygen minimum zones (OMZs) in the modern ocean. Prog. Oceanogr. 80, 113–128. doi:10.1016/j.pocean.2008.08.001

Plank, W.S., Pak, H., Zaneveld, J.R.V., 1972. Light scattering and suspended matter in nepheloid layers. Journal of Geophysical Research 77, 1689–1694. doi:10.1029/jc077i009p01689

Pörtner, H.O., Farrell, A.P., 2008. Physiology and Climate Change. Science 322, 690–692. doi: 10.1126/science.1163156

Postma, D., Jakobsen, R., 1996. Redox zonation: Equilibrium constraints on the Fe(III)/SO4-reduction interface. Geochimica et Cosmochimica Acta 60, 3169–3175. doi:10.1016/0016-7037(96)00156-1

Prince, E.D., Goodyear, C.P., 2006. Hypoxia-based habitat compression of tropical pelagic fishes. Fish. Oceanogr. 15, 451–464. doi:10.1111/j.1365-2419.2005.00393.x

Prokopenko, M., Sigman, D., Berelson, W., Hammond, D., Barnett, B., Chong, L., Townsend-Small, A., 2011. Denitrification in anoxic sediments supported by biological nitrate transport. Geochimica et Cosmochimica Acta 75, 7180–7199. doi:10.1016/j.gca.2011.09.023

Reimers, C. E., M. Kastner, And R. E. Garrison., 1990. The role of bacterial mats in phosphate mineralization with particular reference to the Monterey Formation, p. 300-311. In W. C. Burnett and S. R. Riggs [eds.], Phosphate deposits of the world. V. 3. Cambridge.

Røy, H., Weber, H.S., Tarpgaard, I.H., Ferdelman, T.G., Jørgensen, B.B., 2014. Determination of dissimilatory sulfate reduction rates in marine sediment via radioactive35S tracer. Limnology and Oceanography: Methods 12, 196–211. doi:10.4319/lom.2014.12.196

Savrda, C. E., Bottjer, D. J., Gorsline, D. S., 1984. Development of a Comprehensive Oxygen-Deficient Marine Biofacies Model: Evidence from Santa Monica, San Pedro, and Santa Barbara Basins, California Continental Borderland. AAPG Bulletin 68. doi:10.1306/ad4616f1-16f7-11d7-8645000102c1865d

Schmidtko, S., Stramma, L., Visbeck, M., 2017. Decline in global oceanic oxygen content during the past five decades. Nature 542, 335–339. doi:10.1038/nature21399

Severmann, S., Mcmanus, J., Berelson, W.M., Hammond, D.E., 2010. The continental shelf benthic iron flux and its isotope composition. Geochimica et Cosmochimica

Acta 74, 3984–4004. doi:10.1016/j.gca.2010.04.022

Sorokin, Y. I. 1962. Experimental investigation of bacterial sulfate reduction in the Black Sea using S^{35}. Microbiology (Engl. Transl.), 31: 329–335.

Stramma, L., Johnson, G.C., Sprintall, J., Mohrholz, V., 2008. Expanding Oxygen-Minimum Zones in the Tropical Oceans. Science 320, 655–658. doi:10.1126/science.1153847

Stramma, L., Schmidtko, S., Levin, L.A., Johnson, G.C., 2010. Ocean oxygen minima expansions and their biological impacts. Deep. Res. Part I Oceanogr. Res. Pap. 57, 587–595. doi:10.1016/j.dsr.2010.01.005

Sturdivant, S.K., Díaz, R.J., Cutter, G.R., 2012. Bioturbation in a declining oxygen environment, in situ observations from wormcam. PLoS One 7. doi:10.1371/journal.pone.0034539

Treude, T., Niggemann, J., Kallmeyer, J., Wintersteller, P., Schubert, C.J., Boetius, A., Jørgensen, B.B., 2005. Anaerobic oxidation of methane and sulfate reduction along the Chilean continental margin. Geochimica et Cosmochimica Acta 69, 2767–2779. doi:10.1016/j.gca.2005.01.002

Treude, T., Krause, S., Maltby, J., Dale, A.W., Coffin, R., Hamdan, L.J., 2014. Sulfate reduction and methane oxidation activity below the sulfate-methane transition zone in Alaskan Beaufort Sea continental margin sediments: Implications for deep sulfur cycling. Geochimica et Cosmochimica Acta 144, 217–237. doi:10.1016/j.gca.2014.08.018

Vaynshteyn, M. B., Tokarev, V. G., Shakola, V. A., Lein, A. Y., Ivanov, M. V., 1985. The geochemical activity of sulfate-reducing bacteria in sediments in the western part of the Black Sea. Geokhimiya (Engl. Transl.), 7, 1032-1044.

Wallmann, K., 2010. Phosphorus imbalance in the global ocean? Global Biogeochemical

Cycles 24. doi:10.1029/2009gb003643

Wallmann, K. 2003. Feedbacks between oceanic redox states and marine productivity: A model perspective focused on benthic phosphorus cycling. Glob. Biogeochem. Cycles 17: 1084, doi:10.1029/2002GB001968

Wenzhöfer, F., Glud, R.N., 2002. Benthic carbon mineralization in the Atlantic: a synthesis based on in situ data from the last decade. Deep Sea Research Part I: Oceanographic Research Papers 49, 1255–1279. doi:10.1016/s0967-0637(02)00025-0

Wright, J.J., Konwar, K.M., Hallam, S.J., 2012. Microbial ecology of expanding oxygen minimum zones. Nature Reviews Microbiology. doi:10.1038/nrmicro2778